Research Square

Preprints are preliminary reports that have not undergone peer review.
They should not be considered conclusive, used to inform clinical practice,
or referenced by the media as validated information.

Therapeutic ultrasound enables rapid and robust activation of ROS-responsive prodrugs in vivo

Guoquan Liu

guoquanliu@bjmu.edu.cn

Peking University https://orcid.org/0000-0003-0680-4811

Shuyu Huan

Peking University

Zixi Li

Peking University

Tianzhen Sun

Peking University

Bingru Li

Peking University

Xunbin Wei

Peking University

Xiaoda Yang

Peking university

Article

Keywords:

Posted Date: June 22nd, 2026

DOI: https://doi.org/10.21203/rs.3.rs-9984684/v1

License: This work is licensed under a Creative Commons Attribution 4.0 International License.
Read Full License

Additional Declarations: There is **NO** Competing Interest.

Therapeutic ultrasound enables rapid and robust activation of ROS-responsive prodrugs in vivo

Shuyu Huan[#,1,2], Zixi Li[#,2,3], Tianzhen Sun[#,4], Bingru Li[1], Xunbin Wei[2,3,4,5], Xiaoda Yang[1], Guoquan Liu[2,3*]

[1] Department of Chemical Biology, School of Pharmaceutical Sciences, Peking University, Beijing 100191, China

[2] Beijing Key Laboratory of Medical-Engineering Integration and Translation for Malignant Tumours, Institute of Advanced Clinical Medicine, Peking University, Beijing, 100191, China.

[3] Center of Biomedical Engineering, Institute of Advanced Clinical Medicine, Peking University, Beijing 100191, China

[4] Institute of Medical Technology, Peking University Health Science Center, Beijing, 100191, China

[5] Key laboratory of Carcinogenesis and Translational Research (Ministry of Education/Beijing), Peking University Cancer Hospital & Institute, Beijing, 100142, China

* Corresponding author：guoquanliu@bjmu.edu.cn (G. Liu).

# Contributed equally.

Abstract

Reactive oxygen species (ROS)-responsive prodrugs offer a route to disease-selective drug activation, but their in vivo performance is often constrained by heterogeneous ROS production, short ROS lifetimes and reductive quenching. Therapeutic ultrasound can generate reactive species locally and on demand in deep tissues, yet whether conventional ROS-responsive masking groups respond productively to sonochemical activation and enable efficient drug release remains unclear. Here we show that, among representative ROS-responsive triggers, boronic acid/boronate motifs emerge as the most productive ultrasound-responsive motifs for prodrug activation, enabling rapid, robust and programmable release. Mechanistic studies indicate that this performance arises from a mixed sonochemical oxidation regime, in which hydrogen peroxide serves as the longer-lived oxidant and sustains major boronate oxidation, while transient hydroxyl radicals provide additional contributions. We validate this strategy using fluorogenic probes, doxorubicin and monomethyl auristatin E (MMAE) prodrugs, and an albumin–MMAE conjugate. In tumour-bearing mice, localized ultrasound enables therapeutic activation of boronic acid/boronate-caged prodrugs within short irradiation windows, suppressing tumour growth while reducing systemic toxicity. These findings establish therapeutic ultrasound as an external trigger for spatiotemporally controlled prodrug activation in vivo and provide design principles for advancing ROS-responsive prodrug chemistry beyond the constraints of endogenous ROS activation.

Introduction

Stimuli-responsive prodrugs and masked functional molecules offer a powerful route to widen the therapeutic window of potent therapeutics by restricting activity to diseased tissues[1]. In practice, however, achieving bond cleavage on demand, at depth, and with molecular precision remains a major challenge. Many activatable systems rely on endogenous tumour microenvironment cues, such as acidic pH, hypoxia, enzyme overexpression or altered redox balance[2], but these biochemical triggers are highly heterogeneous across tumour types and disease stages, often leading to

premature activation or incomplete release[3]. Reactive oxygen species (ROS)-responsive prodrugs exemplify this challenge. Although oxidative stress is widely exploited for disease-selective activation, endogenous ROS signals are heterogeneous, low in steady-state abundance and readily buffered by reductive biological environments[4-6]. Moreover, the oxidative trigger available in a given lesion may not match the activation threshold, oxidant selectivity or release kinetics of a given ROS-responsive motif[7,8]. Consequently, chemically well-established ROS-responsive triggers may not translate into reliable, spatially controlled prodrug activation in vivo[9]. Exogenous activation strategies that can provide precise spatial and temporal control are therefore of considerable interest[10].

Among external triggers, ultrasound is uniquely attractive because it combines deep tissue penetration, noninvasiveness, clinical compatibility and spatiotemporal addressability[11,12]. Yet converting acoustic energy into selective small-molecule bond activation remains difficult[13,14]. To date, many ultrasound-mediated systems have relied on mechanical effects[15-17], carrier disruption[18,19], thermal effects[20] or sonodynamic therapy[21-24], all of which can impose constraints such as dependence on bulky delivery vehicles[25,26], sonosensitizers[27] or oxygen availability[28]. Recent examples of ultrasound-activatable masking groups have shown that acoustic cavitation can be harnessed for direct molecular uncaging[29-32]. However, these systems have largely been designed or interpreted around transient radical or radical-derived species, such as hydroxyl radicals (·OH) [29,30,33] and superoxide anions ($O_2{\cdot}^-$)[31,32], generated during water sonolysis (Figure 1a). Because acoustic cavitation produces a mixed sonochemical environment containing both transient radicals and hydrogen peroxide, it remains unclear which ROS-responsive motifs can best convert ultrasound-generated reactivity into productive payload release rather than non-productive degradation. In particular, it remains unresolved whether peroxide-responsive motifs can harness sonochemically generated hydrogen peroxide in the bulk phase to overcome the limited diffusion, rapid quenching and short reaction windows associated with transient-radical activation (Figure 1b).

Here, we sought to identify ROS-responsive masking groups that are not merely

ultrasound-reactive, but ultrasound-productive, and to determine whether bulk-oxidant-supported activation can enable efficient drug release beyond the constraints of endogenous ROS activation. We therefore used productive payload release, rather than trigger consumption alone, as the central criterion to compare representative transient-radical-sensitive and peroxide-responsive motifs under matched therapeutic ultrasound conditions. This design allowed us to test whether ultrasound-triggered uncaging is confined to short-lived radical chemistry or can be extended to a hydrogen peroxide-supported bulk activation mode with improved robustness in reductive and tumour-mimicking environments (Figure 1c). Our screening identified boronic acid/boronate motifs as the most productive ultrasound-responsive triggers among the tested ROS-responsive motifs. Comparative mechanistic studies show that boronic-acid/boronate uncaging is not governed by a hydroxyl-radical-only pathway, but instead by a composite mechanism in which hydrogen peroxide sustains the major productive boronate-oxidation pathway while transient radical contributions reinforce activation.

This mixed activation mechanism enables rapid, robust and irradiation-programmed release in reductive and tumour-mimicking environments. We then translated this trigger chemistry into fluorogenic probes, small-molecule prodrugs and an albumin–drug conjugate to test whether mechanistically selected trigger chemistry remains operative beyond simple molecular scaffolds. In tumour-bearing mice, localized ultrasound activates boronic acid/boronate-caged prodrugs within short irradiation windows, suppressing tumour growth while reducing systemic toxicity. Together, this work establishes therapeutic ultrasound as an external trigger for spatiotemporally controlled ROS-responsive prodrug activation in vivo and provides design principles for advancing ROS-responsive prodrug chemistry beyond the constraints of endogenous ROS activation, from small-molecule prodrugs to macromolecular drug conjugates.

Results and Discussion

1. Representative screening identifies chemically useful ultrasound-responsive

masking groups

Acoustic cavitation generates a complex ROS environment containing both transient radicals and hydrogen peroxide as the longer-lived oxidant[34], as confirmed by EPR spin-trapping and H_2O_2 quantification experiment (Extended Data Fig. 1b, Supplementary Fig. 1), suggesting that structurally distinct ROS-responsive motifs might undergo uncaging and release payload under ultrasound (Fig. 2a). We therefore performed a representative screening of ROS-responsive candidate masking groups covering hydroxyl-radical-sensitive 3,5-dihydroxybenzyl carbamate (DHBC) motifs[29,30], reduction-sensitive azide derivatives (aryl azides[31,32] and sulfonyl azides), and peroxide-reactive motifs such as boronic acid/boronate groups[33], α-ketoamides[35], oxalates, and pentafluorobenzenesulfonate[36]. Several of these motifs have already been employed in other ROS-generating activation contexts, including X-ray-responsive systems[37-40], but their relative behaviour has not been systematically compared under matched therapeutic ultrasound conditions.

Under a common therapeutic ultrasound condition (1 MHz, 3.0 W cm^{-2}, 70% duty cycle, 3 min, chosen after preliminary sonication-parameter optimization, Extended Data Fig. 1c,d), the tested substrates **1**–**16** (10 μM, 200 μL) displayed marked differences between desired product formation and non-productive degradation (Fig. 2b,c). Among the candidates plausibly activated through radical-mediated pathways, DHBC-type substrates **1**–**3** showed the highest level of ultrasound reactivity as well as productive release rate, with desired-product formation of 16–19% (Fig. 2b,c; Supplementary Fig. 15). Azide-derived substrates **4**–**6** also underwent measurable ultrasound-induced transformation (20–40%), but with substantially lower productive conversion (~3%) than DHBC-type motifs (Supplementary Fig. 12). Sulfonyl azides **7**–**8** showed slightly improved productive conversion (~5%) relative to the simple aryl azides **4**–**6** in the same subset (Supplementary Fig. 13); however, they still underperformed DHBC under the same condition and, since their cleavage chemistry primarily affords sulfonamide products, their utility as a broadly applicable masking group remains intrinsically limited.

A different trend was observed among supposedly peroxide-reactive candidates.

Boronic acid/boronate substrates **9–13** consistently afforded the most favourable product profiles in this subset, with representative desired-product formation exceeding 70% (Fig. 2b,c). By comparison, α-ketoamide and pentafluorobenzenesulfonate substrates showed only modest desired-product formation (<20%) (Supplementary Figs. 14, 17), indicating that peroxide responsiveness in conventional chemical systems does not readily translate into efficient ultrasound-triggered release. The oxalate-based substrate **14** showed a high product-formation ratio among the converted fraction (~80%), but its practical utility was nevertheless severely limited under these aqueous conditions because of pronounced hydrolytic instability (Supplementary Fig. 16).

Taken together, these results show that only a subset of ROS-responsive motifs translate ROS reactivity into chemically useful release behaviour under ultrasound irradiation. The contrasting behaviours of radical-responsive and peroxide-reactive motifs further suggested that the key difference among ultrasound-responsive masking groups may not lie simply in ROS reactivity, but in the sonochemical mode through which productive uncaging is achieved. This hypothesis motivated the mechanistic comparison described below.

2. Distinct sonochemical behaviours explain the productive ultrasound activation of boronic acid/boronate triggers

To test our hypothesis, we selected DHBC- and boronic-acid-type motifs as mechanistically informative representatives of the two best-performing candidates within the radical-responsive and peroxide-reactive subsets, respectively (Fig. 3b, Extended Data Fig. 2a).

We first compared direct substrate irradiation with a delayed-addition protocol (Fig. 3d), in which the aqueous medium was sonicated before the substrate was introduced. This experiment provides an operational distinction between activation that depends on short-lived reactive species generated during cavitation and activation that can be sustained by hydrogen peroxide as the longer-lived oxidant persisting in the bulk phase after sonication. Under delayed-addition conditions, DHBC-type

substrates (10 μM in PBS) showed no detectable conversion (Extended Data Fig. 2b), indicating that productive cleavage requires direct exposure to the cavitation event itself. By contrast, the boronic-acid-type substrate B1 retained substantial reactivity even when added after ultrasound pretreatment of the buffer. In addition, boronic-acid-type substrates continued to show increasing product formation during the post-sonication period (Extended Data Fig. 2c), indicating that a major component of its activation can proceed through hydrogen peroxide generated during sonolysis. These observations immediately suggested that DHBC- and boronic-acid-type motifs are not governed by a shared reactive principle, but instead occupy distinct sonochemical regimes.

To define the reactive species involved in DHBC uncaging, we compared DHBC activation under H_2O_2, Fenton and ultrasound conditions, and examined the effects of radical scavengers during sonication. DHBC cleavage was observed under Fenton reactions but not upon treatment with H_2O_2 alone, and both DMPO and GSH suppressed ultrasound-triggered activation (Extended Data Fig. 2d). Together with the complete loss of reactivity in the delayed-addition experiment, these results indicate that DHBC activation occurs predominantly through highly localized hydroxyl-radical chemistry at or near the cavitation interface[41,42]. We therefore assign DHBC-type activation to a transient interfacial mode, in which productive release is rapid and spatially confined, but intrinsically sensitive to radical quenching and reductive perturbation (Fig. 3a).

To define the reactive species and activation mode involved in boronic-acid uncaging, we used p-hydroxymethylphenylboronic acid (B1) as a model substrate (Fig. 3b). We then compared its behaviour under ultrasound and exogenous H_2O_2 conditions, together with delayed-addition, product-analysis and scavenger-perturbation experiments. Direct ultrasound irradiation rapidly converted B1 into the corresponding phenol B0, whereas treatment with exogenous H_2O_2 at a concentration quantitatively matched to the amount generated during ultrasound irradiation (Extended Data Fig. 1b; Supplementary Figs. 5, 6) failed to reproduce the productive conversion observed under ultrasound (Fig. 3e), indicating that the

ultrasound effect cannot be reduced to simple bulk peroxide addition. This discrepancy became even more pronounced under mildly acidic (Fig. 3f) and reductive (Fig. 3g) conditions, under which H_2O_2-triggered activation was strongly attenuated whereas ultrasound-triggered conversion remained substantial and could be restored to near-complete conversion by prolonging irradiation (Extended Data Fig. 2e). Thus, although a peroxide-supported pathway is clearly operative, these results indicate that bulk peroxide chemistry alone is insufficient to account for the full ultrasound response. LC-MS product analysis further showed that, in addition to the major product B0, ultrasound generated a secondary byproduct Bx that was not reproduced by H_2O_2 treatment alone (Supplementary Fig. 9), suggesting the operation of an additional ultrasound-specific pathway. Scavenger experiments then distinguished the two product branches (Fig. 3i; Extended Data Fig. 2f,g; Supplementary Fig. 10). Hydroxyl-radical scavengers[43] suppressed or completely abolished Bx formation, whereas peroxide quenching reduced B0 production. Notably, IPA decreased Bx formation but increased B0 yield, consistent with its dual role as a hydroxyl-radical scavenger and a promoter of H_2O_2 accumulation[44] under ultrasound (Supplementary Figs. 4–6). Together, these data support a model in which boronic-acid uncaging under ultrasound proceeds predominantly through a peroxide-supported productive pathway, while hydroxyl radicals contribute to the Bx branch and may also contribute to the enhanced ultrasound response through additional transient sonochemical pathways (Fig. 3h).

This mechanistic interpretation is further supported by comparison with other peroxide-reactive motifs screened under the same ultrasound condition. Although α-ketoamide, oxalate and pentafluorobenzenesulfonate are all nominally peroxide-responsive, none matched the productive performance of boronic-acid-type substrates (Fig. 2b,c). This observation suggests that peroxide reactivity alone is not sufficient to ensure efficient ultrasound-triggered uncaging. Instead, the poorer behaviour of these motifs may reflect, at least in part, a greater susceptibility to transient radical-mediated damage during cavitation, potentially arising from structural features that disfavour productive reaction in the bulk solution while

increasing exposure to interfacial degradation pathways. More broadly, these results indicate productive release may require compatibility between the lifetime and localization of sonogenerated species and the reaction pathway of the masking group. Control experiments further excluded purely thermal or pyrolytic pathways for boronic-acid activation. No productive conversion was observed under simple heating or in anhydrous aprotic media, confirming that aqueous ROS generation is essential (Supplementary Figs. 2,3). Comparable trends were also observed for additional boronic-acid substrates, supporting the generality of this activation behaviour within the boronic acid/boronate subset (Supplementary Fig. 11).

Taken together, these data show that productive ultrasound-triggered uncaging is not governed by a single sonochemical mechanism. Instead, at least two mechanistically distinct activation modes can be distinguished. DHBC-type motifs exemplify transient interfacial activation, in which productive cleavage depends on short-lived radical chemistry confined to the cavitation interface (Fig. 3a). By contrast, boronic-acid-type motifs exemplify persistent bulk activation, in which productive release is sustained primarily by hydrogen peroxide as the longer-lived oxidant in solution while remaining reinforced by transient radical contributions (Fig. 3h). This mechanistic distinction provides a basis for understanding why only a subset of ROS-responsive motifs emerge as practically useful and robust ultrasound triggers.

3. Composite sonochemical activation enables robust and programmable molecular release in complex biological environments

The mechanistic distinction defined above suggested that boronic-acid-caged substrates should be especially well suited to productive release in chemically and biologically complex environments (Fig. 4a). We therefore asked whether this advantage could be translated into functional molecular release using fluorogenic probes as direct readouts of productive uncaging (Fig. 4b). In CB, boronate oxidation is followed by 1,6-elimination to generate the fluorogenic product. In MRB, boronate oxidation and 1,6-elimination are followed by carbamate cleavage to release the fluorescent product (Supplementary Figs. 20,21). Under in vitro ultrasound irradiation

(1 MHz, 3.0 W cm^{-2}, 70% duty cycle), both probes (10 μM in PBS) showed efficient turn-on responses in PBS, as confirmed by fluorometric and HPLC analyses, indicating that boronic-acid-mediated uncaging remains effective across chemically distinct release formats (Extended Data Fig. 3a–g).

We next examined whether ultrasound-triggered boronic-acid activation retained functional efficiency under certain biological conditions that suppress conventional peroxide-mediated triggering. CB was therefore evaluated in PBS, in reductive medium (DMEM + 10% FBS + 1 mM GSH), and in mildly acidic tumour cell lysate (pH 6.5). Under reductive and tumour-mimicking conditions, activation by exogenous H_2O_2 and other defined exogenous ROS/RNS stimuli was strongly attenuated, whereas ultrasound maintained substantial fluorogenic release (Fig. 4c,d; Extended Data Fig. 3j–n; Extended Data Fig. 3h,i). These data show that ultrasound maintains productive boronic-acid uncaging under chemically challenging conditions in which exogenous peroxide triggering is strongly attenuated.

This distinction was also evident kinetically. For MRB, ultrasound-triggered activation proceeded more rapidly than treatment with exogenous H_2O_2, even though the externally supplied H_2O_2 concentration far exceeded that generated during sonication (Fig. 4e; Extended Data Fig. 1b). This comparison is particularly informative because boronate oxidation by H_2O_2 is kinetically favoured under more alkaline conditions, whereas the near-neutral assay conditions used here render direct peroxide triggering relatively sluggish. Ultrasound in contrast did not show the same limitation. Thus, the functional advantage of ultrasound lies not only in maintaining activation in hostile media, but also in accelerating productive release relative to peroxide alone.

We then examined whether ultrasound-triggered boronic-acid activation remained chemically discriminating and externally controllable. In competitive experiments, CB was incubated together with structurally related unprotected coumarin derivatives that are themselves susceptible to hydroxyl-radical-mediated degradation (Supplementary Fig. 28). Under brief ultrasound exposure, cleavage of the boronic-acid-caged probe clearly predominated, whereas degradation of the

unprotected coumarins remained limited (Fig. 4f). Productive uncaging is therefore not simply a consequence of indiscriminate oxidative destruction. The same trigger chemistry also remained temporally programmable. Repeated on/off irradiation cycles produced a stepwise increase in fluorescence from CB, demonstrating that ultrasound-triggered molecular release remains tightly coupled to the external ultrasound input and can be regulated in time (Fig. 4g). Together, these results show that ultrasound-triggered boronic-acid uncaging remains both chemically selective and temporally programmable.

Having established these functional advantages in solution, we next examined whether the same trigger chemistry remained operative in living systems. In MDA-MB-231 cells, in situ sonication after incubation with CB produced a clear ultrasound-duration-dependent increase in fluorescence by flow cytometry, whereas untreated or non-sonicated controls showed minimal activation (Fig. 4h). Confocal imaging likewise visualized intracellular fluorescence generation after ultrasound exposure (Extended Data Fig. 4b), and MRB displayed the same qualitative behaviour, with signal intensity increasing with probe concentration and irradiation duration (Fig. 4i; Extended Data Fig. 4c). Finally, MRB was administered intratumourally in 4T1 tumour-bearing mice, followed by localized ultrasound irradiation, and tumour sections were analysed ex vivo (Fig. 4j; Extended Data Fig. 4d,e). Ultrasound-treated groups showed markedly stronger fluorescence than non-sonicated controls, with signal intensity increasing with irradiation duration, confirming that boronic-acid-caged probes remain activatable in live tumour tissue.

Together, these probe-based studies show that boronic-acid-caged probes remain functional across solution, cellular and tumour-associated settings, supporting its use as a robust ultrasound-responsive trigger for biological applications.

4. Ultrasound-triggered activation enables controlled small-molecule prodrug chemotherapy

Guided by the mechanistic and probe-level validation above, we next asked whether the same trigger chemistry could support the controlled release of a

therapeutically relevant small-molecule payload. Doxorubicin (Dox) was selected as an initial model because of its potent antitumour activity and well-recognized dose-limiting systemic toxicity. We therefore prepared the boronic-acid-caged Dox prodrug DB and examined whether the same trigger chemistry that enabled robust probe activation could be translated into controlled chemotherapy (Fig. 5a). As an initial step, we compared the precursor stability of DB with that of the corresponding DHBC-caged analogue DD under biologically relevant conditions (Extended Data Fig. 5q). DB showed a more advantageous stability profile in cell culture medium and plasma, further supporting its selection for downstream therapeutic validation.

Under established acoustic parameters, DB (10 μM in PBS) underwent time-dependent conversion to free Dox, as confirmed by HPLC analysis (Fig. 5b–c). These data show that the boronic-acid trigger remains competent for productive uncaging when coupled to a clinically relevant small-molecule drug. To determine whether the released payload retained biological activity, we first performed ex situ activation experiments, in which DB was sonicated before addition to cells. Across six tumour cell lines, ultrasound-preactivated DB showed markedly enhanced cytotoxicity relative to non-sonicated DB (approximately 20-fold) and approached the activity of free Dox, demonstrating efficient drug release (Fig. 5d; Extended Data Fig. 5a–d).

We then examined whether activation could also be achieved directly in the presence of intact cells under cell-compatible ultrasound conditions. In situ sonication (1.0 W cm^{-2}, 10% duty cycle, 5 min) of 4T1 cells incubated with DB produced pronounced, dose-dependent cytotoxicity, whereas DB alone or ultrasound alone caused minimal cell death (Fig. 5e; Extended Data Fig. 5e–h). Thus, the boronic-acid trigger not only releases Dox efficiently in solution, but also remains functional under biologically compatible irradiation conditions.

The therapeutic relevance of this chemistry was next examined in vivo in 4T1 tumour-bearing Balb/c mice. DB was administered intraperitoneally at doses equivalent to 1× (6.9 mg/kg, marked as DB-low) or 3× (20.7 mg/kg, marked as DB-high) the molar amount of Dox (5 mg/kg), followed by localized ultrasound at

defined time points post injection (Fig. 5f). DB alone showed little antitumour activity, whereas DB + US markedly suppressed tumour growth and reduced endpoint tumour weight (Fig. 5g,h). Importantly, this therapeutic benefit was achieved with substantially improved tolerability relative to free Dox. Whereas Dox-treated mice exhibited pronounced body-weight loss (>20%) and histological evidence of systemic toxicity, DB + US–treated animals maintained significantly better weight stability and showed reduced organ damage (Fig. 5i; Extended Data Fig. 5i–m; Supplementary Fig. 26). Acute-toxicity evaluation further confirmed that high-dose DB combined with ultrasound was substantially better tolerated than the corresponding free-drug treatment (Supplementary Fig. 25). Finally, a head-to-head in vivo comparison between the DHBC- and boronic-acid-caged Dox prodrugs further illustrated the distinct in vivo therapeutic effects of transient interfacial and persistent-bulk-dominated activation (Extended Data Fig. 5r). Under otherwise matched dose and ultrasound treatment, DB afforded stronger tumour suppression than DD, consistent with the greater environmental robustness of a persistent-bulk-dominated activation mode in vivo**.**

Collectively, these results show that the mechanistically selected boronic-acid trigger can be translated from fluorogenic probes to therapeutically relevant small-molecule prodrugs. In this setting, ultrasound enables controlled release of a clinically important cytotoxic agent with an improved balance between efficacy and tolerability.

5. Ultrasound-triggered activation extends to potent payloads and an albumin–drug conjugate format

We next asked whether the same trigger chemistry could be extended beyond a single small-molecule chemotherapeutic to more potent payloads and, ultimately, to more advanced therapeutic formats. To address this, we selected monomethyl auristatin E (MMAE), a highly potent tubulin inhibitor whose clinical utility is generally restricted to targeted delivery systems because of its extreme systemic toxicity[45]. A boronic-acid-caged MMAE prodrug, MB, was therefore prepared to test

whether ultrasound-triggered activation could be generalized to a structurally and pharmacologically distinct payload (Fig. 6a).

As with DB, MB (50 μM in PBS) underwent efficient ultrasound-triggered conversion to free MMAE in PBS, as shown by HPLC analysis (Fig. 6b). Ex situ activation experiments in 4T1 and MDA-MB-231 tumour cells showed that ultrasound-pretreated MB acquired cytotoxicity approaching that of free MMAE, confirming productive release of the active payload (Fig. 6c; Extended Data Fig. 6a). In situ experiments further demonstrated functional activation in a biological context. Under cell-compatible sonication conditions (1.0 W cm^{-2}, 10% duty cycle, 5 min), MB + US markedly inhibited tumour-cell migration in wound-healing assays, whereas MB alone showed limited effect (Fig. 6d; Extended Data Fig. 6b; Supplementary Fig. 24). These data indicate that the boronic-acid trigger remains operative even when coupled to a highly potent payload with a very narrow therapeutic window.

We then evaluated this strategy in 4T1 tumour-bearing mice. Intravenous administration of MB (0.68 mg/kg; MMAE-equivalent 0.5 mg/kg) followed by localized ultrasound significantly suppressed tumour growth and reduced endpoint tumour burden relative to control groups (Fig. 6e–g). Although free MMAE also showed strong antitumour activity, it was accompanied by clear systemic toxicity. By contrast, MB + US achieved therapeutic benefit with a more favourable safety profile, as reflected in body-weight monitoring (Fig. 6h), blood biochemistry (Extended Data Fig. 6d–i) and histological evaluation (Supplementary Fig. 27). Long-term survival analysis further showed that MB + US prolonged survival relative to untreated controls and compared favourably with the free-drug group (Fig. 6i), supporting the conclusion that ultrasound-triggered boronic-acid activation can harness highly potent cytotoxins while mitigating systemic burden.

To determine whether the same trigger chemistry remains operative not only across payloads but also across therapeutic formats, we finally incorporated it into an albumin–drug conjugate. The resulting sono-caged BSA–MMAE conjugate, BSA-L1101, was designed as a higher-order therapeutic construct in which the

boronic-acid trigger is embedded within a macromolecular delivery architecture (Fig. 6j, Extended Data Fig. 6n). Under ultrasound, BSA-L1101 underwent productive activation to release MMAE, extending boronic-acid-triggered uncaging to the conjugated state. In vitro, ultrasound-treated BSA-L1101 showed substantial cytotoxicity across multiple tumour cell lines, whereas the non-sonicated conjugate remained much less effective (Fig. 6k; Extended Data Fig. 6j–m).

In a 4T1 tumour-bearing nude mouse model, intravenous BSA-L1101 was administered every three days, with each dose followed by multiple localized ultrasound exposures at defined post-injection intervals. This schedule was designed to separate systemic prodrug administration from local payload activation, allowing repeated ultrasound-programmed release from a macromolecular conjugate rather than immediate burst release after injection. BSA-L1101 combined with localized ultrasound significantly inhibited tumour growth and reduced endpoint tumour weight (Fig. 6l,m). This therapeutic effect was achieved with acceptable tolerability, as reflected by body-weight changes and organ-level readouts (Extended Data Fig. 6n–p).

Taken together, these studies extend the same externally controlled activation principle from small-molecule prodrugs to a macromolecular drug conjugate, supporting a generalizable strategy for spatially and temporally controlled payload release. Uniquely, the macromolecular conjugate design decouples systemic circulation from local activation and allows repeated ultrasound-defined release windows. This conjugate-level validation further points to the potential of mechanistically selected ultrasound-responsive triggers for more advanced bioconjugate formats, including ADC-inspired therapeutic designs.

Conclusion

In summary, this study repositions therapeutic ultrasound from a physical drug-delivery trigger to a chemically programmable source of localized oxidative stimuli for activating ROS-responsive prodrugs in vivo, shifting prodrug activation from reliance on heterogeneous endogenous ROS to localized sonochemical reactivity.

This strategy addresses a central limitation of conventional ROS-responsive prodrug activation, in which release depends on pre-existing ROS signals that are often insufficient, spatially variable or poorly matched to the activation threshold of a given masking group.

By comparing representative ROS-responsive masking groups under matched ultrasound conditions, we show that conventional ROS responsiveness does not necessarily translate into useful ultrasound responsiveness. Several ROS-reactive motifs undergo inefficient release or competing degradation, whereas boronic acid/boronate motifs emerge as the most productive ultrasound-responsive triggers among the tested motifs for productive cargo release. These findings define a sonochemical trigger-matching principle for ROS-responsive prodrug activation that productive release depends on matching sonogenerated reactivity with the intrinsic reaction pathway and degradation susceptibility of the masking group.

Mechanistically, our results distinguish two sonochemical activation behaviours. DHBC-type motifs primarily depend on transient interfacial radical chemistry, whereas boronic acid/boronate motifs exploit a mixed oxidation regime in which hydrogen peroxide sustains the major boronate oxidation pathway and transient hydroxyl radicals provide reinforcing contributions. This composite mechanism explains the rapid activation, high release efficiency and robustness of boronic acid/boronate triggers in reductive and tumour-mimicking environments, and enables irradiation-programmed release under therapeutic ultrasound.

The utility of this trigger chemistry extends from fluorogenic probes to doxorubicin and MMAE prodrugs, as well as an albumin–MMAE conjugate. In tumour-bearing mice, localized ultrasound activates boronic acid/boronate-caged prodrugs within short irradiation windows, suppressing tumour growth while reducing systemic toxicity. Together, these findings define a sonochemical design principle for advancing ROS-responsive prodrug chemistry beyond endogenous ROS activation and support therapeutic ultrasound as a precision trigger for spatiotemporally controlled prodrug activation in vivo across small-molecule prodrugs and macromolecular drug conjugates.

Methods

Reagents and apparatus

Chemical reagents were purchased from Sigma-Aldrich, J&K and Alfa Aesar. All chemicals were used as received without further purification unless otherwise stated. Sono-responsive caged compounds (designated as Compounds **1–22**, see Supplementary Tab. 1–4) were synthesized, purified, and characterized according to procedures detailed in the Experimental Section of the Supplementary Information. Cell culture reagents including Dulbecco's Modified Eagle Medium (DMEM), RPMI-1640 Medium, fetal bovine serum (FBS), penicillin, and streptomycin were obtained from Gibco (Thermo Fisher Scientific, USA). 3-(4,5-Dimethylthiazol-2-yl)-2,5-diphenyltetrazolium bromide (MTT) was purchased from Beyotime Biotechnology Institute (China). Ultrapure water (resistivity 18.2 $M\Omega\,cm^{-1}$) was prepared using a Milli-Q Reference water purification system (Millipore, USA).

Ultrasound irradiation was carried out using a Nu-Tek UT1021 ultrasonic device with a 1 cm^2 transducer probe, with adjustable parameters (frequency $f = 1$ or 3 MHz, power intensity $I_P = 0\text{-}3.0\ W\,cm^{-2}$ and duty cycle DC=10-100%). Nuclear magnetic resonance (NMR) spectra were recorded on a Bruker AVANCE III 400 MHz spectrometer using deuterated solvents obtained from Sigma-Aldrich. MestReNova v.7 was used for NMR analysis. Signals are presented as parts per million (ppm) and multiplicity is presented as single (s), broad (b), doublet (d), triplet (t), quartet (q) or multiplet (m). Analytical HPLC assays were performed on a Shimadzu LC-20 ADXR system with an Agilent ZORBAX SB-C18 column (4.6 × 250 mm, 5 μm, column temperature 40 °C) and a Shimadzu Nexera SPD-M40 PDA Detector. Preparative HPLC separations were performed via an Elite EClassical 3140 semi-preparative system equipped with an Agilent C18 column (20 × 250 mm, 5 μm) at a flow rate of 10 mL/min. Ultra-performance liquid chromatography–mass spectrometry (UPLC–MS) was performed on a Thermo Ultimate 3000 nano LC system equipped with a

Thermo Q Exactive HF-X Hybrid Quadrupole-Orbitrap mass spectrometer. High-resolution mass spectroscopy was performed on a Waters Xevo G2-S Q-ToF Mass Spectrometer. Electron paramagnetic resonance (EPR) signals were detected using a Bruker ELEXSYS E 580 spectrometer. Fluorescence spectra were measured on an Agilent Cary Eclipse spectrometer. Microplate reading was performed using an Agilent BioTek Synergy NeO_2 Multi-Mode Reader. Flow cytometry analysis was performed on a Beckman Coulter Cytoflex LX flow cytometer. Confocal fluorescence images were recorded on a Leica STELLARIS 8 STED confocal microscope platform equipped with Leica HyD X detectors. Data were analysed and plotted using Origin 2020 (OriginLab) or GraphPad Prism 9 (GraphPad Software). BioRender was used to design some of the illustration in the manuscript and Supporting Information (https://biorender.com).

Syntheses of sono-responsive caged compounds

Full synthetic procedures can be found in Supplementary Information.

Sonication experiments

As shown in Extended Data Fig. 1a, in vitro sonication was carried out with sonication frequency $f = 1$ MHz, power intensity $I_P = 3.0$ W cm^{-2} and duty cycle $DC =$ 70%. Caged compounds were dissolved in DMSO:1× PBS (v:v= 1:1000) to a final concentration of 10 μM unless otherwise stated. For each in vitro trial, 200 μL of the mixture was transferred to a sample tube (borosilicate glass, 11.6 mm × 32 mm), exposed to ultrasound irradiation for designated durations, with aliquots collected at specific time points for fluorescence spectroscopy and HPLC analysis.

Ex situ sonication was conducted under identical ultrasonic parameters to the in vitro experiments. Caged compounds were dissolved in complete cell culture medium. For each ex situ trial, 2 mL of the solution was taken out and placed in a sample bottle (borosilicate glass, 14 mm × 47 mm), where it received ultrasound irradiation for a given time and was then administered to cells for MTT proliferation assays.

In situ sonication employed reduced acoustic parameters ($f = 1$ MHz,

I_P = 1.0 W cm^{-2}, DC = 10%) to minimize direct ultrasound-induced cellular damage. Cultured cells in 12-well plates were incubated with the caged compound-containing medium and exposed to direct sonication through the plate bottom using the stated parameters. Following ultrasound treatment, cells were incubated at 37 °C in a 5% CO_2 incubator for 48/4/4 h before being processed for MTT assay, flow cytometry analysis or confocal microscopy imaging.

In vivo sonication on tumour-bearing mice utilized sonication frequency f = 1 MHz, power intensity I_P = 2.5 W cm^{-2} and duty cycle DC = 70%. Acoustic coupling gel was applied to the tumour site prior to transducer probe placement for ultrasound treatment.

During all sonication experiments, the temperature was maintained at 25-30 °C with a cooling system.

Electron paramagnetic resonance (EPR) detection of ultrasound-generated reactive oxygen species (ROS)

Two types of ROS (hydroxyl radicals ·OH and singlet oxygen $^1O_2$) generated during in vitro sonication were directly quantified using an X-band EPR spectrometer with the spin-trapping method[46]. Spin trapping was performed at 298 K with 4-hydroxy-2,2,6,6-tetramethylpiperidine (4-OH-TEMP, a final concentration of 150 mM in PBS) for $^1O_2$ detection and 5,5-Dimethyl-1-pyrroline N-oxide (DMPO, a final concentration of 200 mM in PBS) for ·OH detection. For in vitro sonication experiments, reaction mixtures (200 μL in borosilicate tubes) were irradiated under standard parameters (1 MHz, 3.0 W cm^{-2}, 70% DC). At designated timepoints, aliquots (30 μL) were immediately transferred to quartz capillaries for EPR measurement. Quantification of spin concentrations was achieved by comparing double-integrated signal intensities against a 4-OH-TEMPO (2,2,6,6-tetramethyl-4-piperidinol-N-oxyl) calibration curve (0.1-100 μM in PBS, R^2 > 0.98). In ROS scavenging studies, glutathione (GSH, final concentrations of 1,5,10 and 20 mM in PBS) was added before sonication. Typical settings applied for EPR detection were: center field, 3510.00 G; scan range, 200.0 G; sweep time, 180.32640 s;

563 modulation amplitude, 1.00 G; modulation frequency, 100.00 kHz; and microwave
564 power, 23.77 mW.
565
566 Quantification of ultrasound-generated hydrogen peroxide (H_2O_2)
567 Ultrasound-generated H_2O_2 was quantified through two independent methods:
568 (I) Iodometric Spectrophotometry. The triiodide (I_3^-) formation method was
569 adapted from Kormann et al. with modifications. In vitro sonicated samples (100 μL
570 aliquots, collected at designated time intervals) were transferred to 96-well plates
571 containing 37.5 μL of 0.1 M potassium hydrogen phthalate buffer and 37.5 μL of a
572 solution containing 0.4 M potassium iodide, 0.06 M sodium hydroxide, and 0.1 mM
573 ammonium molybdate. After 2 min incubation (37 °C, dark conditions), absorbance at
574 352 nm was measured using a microplate spectrophotometer. H_2O_2 concentrations
575 were calculated via external calibration (0-1000 μM H_2O_2 standards in PBS).
576 (II) Amplex Red/horseradish peroxidase (HRP) assay. Following manufacturer's
577 protocol (Thermo Fisher A22188) with minor modifications, 100 μL of in vitro
578 sonicated samples were mixed with 4.0 μL of 10 mM Amplex Red stock solution in
579 DMSO and 1.0 μL of 200 U/mL HRP stock solution. After 2 min incubation (37 °C,
580 dark conditions), fluorescence ($\lambda_{ex}/\lambda_{em}$ = 571/585 nm) and absorption at OD_{560} was
581 measured. H_2O_2 concentrations were quantified through a standard curve.
582 All assays were performed with three independent replicates. In ROS scavenging
583 studies, ROS scavengers were added before sonication. Under hypoxic conditions, the
584 solution was saturated with inert gas in advance, and the inert gas atmosphere was
585 maintained during the ultrasonic process.
586
587 HPLC analysis
588 HPLC separations involved mobile phases of 0.1% (v/v) TFA in ultrapure water
589 (solvent A), 0.1% (v/v) TFA in methanol (solvent B) and 0.1% (v/v) TFA in
590 acetonitrile (solvent C).
591 To analyse the reaction efficiency of compounds **1**–**22** under US radiation and
592 the effects of various radical scavengers on the reaction, the solvent gradient for

HPLC is as follows: 90% solvent A + 10% solvent B (0-3 min), 10-25% solvent B (3-7 min), 25% solvent B (7-10 min), 25-40% solvent B (10-15 min), 90% solvent A + 10% solvent B (15-18 min). The injection volume was 10 μL. The flow rate of 1.2 mL/min.

To analyse the reaction efficiency of compound **19** under US radiation, the solvent gradient for HPLC is as follows: 35% solvent A + 65% solvent B (0-3 min), 65-85% solvent B (3-10 min), 85% solvent B (10-13 min), 35% solvent A + 65% solvent B (13-18 min). The injection volume was 10 μL. The flow rate of 1.0 mL/min.

To analyse the reaction efficiency of compounds **10**–**11**, **15**–**17** under US radiation, the solvent gradient for HPLC is as follows: 20% solvent A + 80% solvent B (0-3.5 min), 80-90% solvent B (3.5-8.5 min), 90% solvent B (8.5-13 min), 20% solvent A + 80% solvent B (13-15 min). The injection volume was 10 μL. The flow rate of 1.0 mL/min.

To analyse the reaction efficiency of compound **18** under US radiation, the solvent gradient for HPLC is as follows: 60% solvent A + 40% solvent C (0-3 min), 40-90% solvent C (3-3.5 min), 90% solvent C (3.5-11.5 min), 60% solvent A + 40% solvent C (11.5-15 min). The injection volume was 10 μL. The flow rate of 1.2 mL/min.

To analyse the reaction efficiency of compounds **20**–**22** under US radiation, the solvent gradient for HPLC is as follows: 60% solvent A + 40% solvent C (0 min), 40-90% solvent C (0-15 min), 60% solvent A + 40% solvent C (15-20 min). The injection volume was 10 μL. The flow rate of 1.2 mL/min.

In HPLC analysis, the consumption of caged compounds and the release of payloads were measured. External standard method was used for quantifying analytes.

UPLC–MS methods

The crude reaction was analysed by UPLC–MS for the identification of reaction intermediates and the study of ultrasound-induced release mechanism. In vitro sonication was carried out according to procedures detailed in the “Sonication experiments” section. Post in vitro sonication, reaction mixtures in PBS were

collected and desalted, freeze-dried into solids, and re-dissolved in a small amount of methanol to obtain a concentrated reaction solution for UPLC–MS detection.

In vitro ultrasound activation of caged fluorescent probes

To demonstrate the feasibility of ultrasound-induced probe activation, two caged fluorophores were used: CB (coumarin-derived) and MRB (methyl rhodol-based). Stock solutions (10 mM in anhydrous DMSO) of caged fluorescent probes were diluted to 10 μM in PBS (DMSO:PBS = 1:1000, v/v). Solutions underwent in vitro sonication according to previously described procedures. Post-sonication aliquots were collected for fluorometric analysis ($\lambda_{ex}/\lambda_{em}$ = 350/500 nm for CB, $\lambda_{ex}/\lambda_{em}$ = 450/520 nm for MRB)as well as HPLC analysis.

In physiological environment simulation experiments, cell lysates (prepared through three freeze-thaw cycles of cell suspensions) and lactic acid supplemented DMEM complete medium (lactic acid, 10 mM, to give a pH of 6.8) supplemented PBS to mimic the intracellular and tumour microenvironment, respectively.

For specificity profiling of CB (10 μM), the responsiveness towards various redox active species (1 mM, 100 e.q.) versus ultrasound treatment was tested using fluorometric analysis. The in vitro ROS/RNS generation method was as follows[32]: (I) ·OH: Hydroxyl radical was generated by Fenton reaction ($[H_2O_2]$:$[Fe^{2+}]$ = 10:1), in which equimolar EDTA was used to avoid the precipitation of Fe(II). The concentration of ·OH was considered equal to the Fe(II) concentration. (II) $^1O_2$: Singlet oxygen was generated from H_2O_2 (1 e.q.) and OCl^- (5 e.q.). (III) ·NO: Nitric oxide was generated from sodium nitroferricyanide(III) dehydrate (SNP, 1 e.q.). (IV) $ONOO^-$: Peroxynitrite solution was prepared from a mixture of sodium nitrite (1 e.q.) and hydrogen peroxide (1 e.q.). (V) $O_2^{\cdot-}$: Superoxide was generated from a mixture of KO_2 (1 e.q.) and H_2O. (VI) H_2O_2: Hydroperoxide solution (1 e.q.) was used directly. (VII) TBHP: Tert-Butyl hydroperoxide solution (1 e.q.) was used directly. (VIII) HOCl: NaOCl solution (1 e.q.) was used directly.

For intracellular interference studies, the experiment was replicated under physiologically relevant GSH concentrations (10 mM GSH in

DMEM complete medium). The response of CB to redox active species or ultrasound treatment under endogenous reducing conditions was evaluated by fluorescence spectroscopy.

Cell culture

All cell lines including 4T1, A375, A549, BT-474, MCF-7, and MDA-MB-231 were purchased from National Infrastructure of Cell Line Resource (Beijing, China). A375, A549 and MCF-7 cells were cultured in Dulbecco's modified Eagle medium (DMEM) supplemented with 10% fetal bovine serum (FBS), 1% penicillin-streptomycin. 4T1, BT-474 and MDA-MB-231 cells were cultured in RPMI-1640 supplemented with 10% FBS, 1% penicillin-streptomycin. All cells were maintained at 37 °C, in a humidified 5% CO_2 incubator, with passage performed every 2-3 days.

In situ ultrasound activation of caged fluorescent probes

MDA-MB-231 cells were seeded in 12-well plates (5×10^5 cells per well) and incubated overnight. Following 30 min pre-incubation with CB (10 μM), direct in situ sonication (0, 1, 3 or 5 min, acoustic parameters as previously described) was performed. Post-treatment cells were incubated for 8 h prior to flow cytometry analysis (λ_{ex}: 405 nm, V525 channel). For MRB activation in situ, the cells were treated with MRB (10 μM) instead, followed by flow cytometry analysis (λ_{ex}: 488 nm, FITC channel). Fluorescence intensity was quantified by FlowJo v10 (FlowJo, LLC). The results are expressed as mean fluorescence ± SD (n = 5).

To visualize the activation of caged fluorescent probes in living cells, MDA-MB-231 cells were seeded in μ-Dish 35 mm dishes (2×10^5 cells/mL) and subjected to identical treatment protocols. In situ sonicated samples were immediately imaged using a confocal microscopy (CB imaging: 405 nm excitation, 430-470 nm emission; MRB imaging: 488 nm excitation, 500-550 nm emission) with 40×/1.30 NA or 63×/1.40 NA oil objectives. Fluorescence quantification encompassed all cellular regions using LAS X Office software (Leica, Germany).

Ex situ ultrasound-activated prodrug cytotoxicity assessment

4T1, A375, A549, BT-474, MCF-7 or MDA-MB-231 cells were seeded in a 96-well plate (3,000-4,000 cells/well) and incubated overnight. Then the culture medium was removed and replaced with 200 μL fresh medium (with 10% FBS) containing caged compounds (DB or MB), free payloads (Dox or MMAE) or caged compounds pre-treated with ex situ ultrasound (3 min, acoustic parameters as previously described). The cells were incubated (for payload Dox, 48 h; for payload MMAE, 72 h) before MTT proliferation assays. The absorbance was measured at 490 nm and all the proliferation data were normalized to the blank control (0.1% v/v DMSO), of which the viability was set as 100%. Measurements were performed with at least three independent replicates.

In situ sonication-activated prodrug cytotoxicity assessment

4T1, A375, A549, BT-474, MCF-7 or MDA-MB-231 cells were seeded in a 12-well plate (5×10^5 cells/well) and incubated overnight. Then the culture medium was removed and replaced with 200 μL fresh medium (with 10% FBS) containing DB at concentrations of 2, 4, 8 and 16 μM or Dox at concentrations of 0.2 and 0.4 μM. Post 30 min incubation, all US groups received in situ sonication (5 min, acoustic parameters as previously described). The cells were incubated for 48 h before MTT proliferation assays as per previously described protocols.

In situ ultrasound-activated prodrug evaluation via wound healing assay

MDA-MB-231 cells were seeded in a 12-well plate (5×10^5 cells/well) and cultured to 100% confluence. Cells were pretreated with fresh medium (with 10% FBS) containing MB (0.2 nM) or MMAE (0.2 nM). Post 30 min incubation, all US groups received in situ sonication (5 min, acoustic parameters as previously described). After 12-h incubation in fresh medium, standardized linear wounds were created across the monolayer using sterile 200 μL pipette tips, with detached cells removed by PBS washing. Cells were maintained in low-serum medium (2% FBS).

Bright field microscopy images were acquired at 0, 12, 24 and 36 h post-wounding. Residual wound area was measured using ImageJ software (NIH) and all the migration data were normalized to the initial 0 h, of which the migration rate was set as 0%. Measurements were performed with three independent replicates.

Tumour model

Female Balb/c mice (7-8 weeks old) from Beijing Vital River Laboratory Animal Technology Co. Ltd. were housed under specific pathogen-free conditions with controlled temperature (20-25°C), humidity (40-70%), 12 h/12 h light/dark cycle, with free access to food and water. Subcutaneous tumours were established by injecting 2×10^6 4T1 cells suspended in 100 μL of PBS into the right flank of mice. Tumour volume (calculated as ($width_2 \times length$)/2) and body weight were measured at least three times per week using digital calipers and an electronic balance, respectively. At the end of the experiment, all the mice were immediately euthanized. Mice were euthanized upon reaching humane endpoints (tumour volume >1,200 mm^3 or >20% body weight loss), with major organs excised for histological analysis (H&E staining) and serum subjected to biochemical profiling.

In vivo ultrasound activation of caged fluorescent probe

When 4T1 tumour volume reached 40-100 mm^3, the tumour-bearing Balb/c mice were randomized into six groups (n = 3): MRB (0.6 mg/kg), MRB + US of indicated durations (0.6 mg/kg + sonication of 2, 4 or 6 min), MR (0.5 mg/kg) and PBS as control. MR (0.5 mg/kg) and MRB (0.6 mg/kg, equivalent to MR concentration of 0.5 mg/kg) were freshly formulated in sterile PBS (5% DMSO, v/v) for intratumoural injection (50 μL/injection). Ultrasound irradiation of indicated durations (procedures and acoustic parameters as previously described) was conducted at the tumour sites 30 min after injection for mice in US groups. To simulate a therapeutic experiment, the treatment cycle (injection followed by sonication) was repeated every 48 h for three administrations. Tumours at the experimental endpoint were harvested for cryosectioning and confocal microscopy imaging.

743

744 In vivo antitumour evaluation of doxorubicin prodrug activation

745 When 4T1 tumour volume reached 40-100 mm^3, the tumour-bearing Balb/c mice
746 were randomized into seven groups (n = 6): Dox (5 mg/kg), Dox + US (5 mg/kg + 2 ×
747 3 min sonication), DB low dose (6.9 mg/kg), DB high dose (20.7 mg/kg), DB low
748 dose + US (6.9 mg/kg + 2 × 3 min sonication), DB high dose + US (20.7 mg/kg + 2 ×
749 3 min US irradiation) and PBS as control. Dox (1 mg/mL, 5 mg/kg) and DB (low dose:
750 1.38 mg/mL, 6.9 mg/kg or high dose: 4.14 mg/mL, 20.7 mg/kg) were freshly
751 formulated in PBS (containing 5% DMSO/40% PEG-300/5% Tween-80, v/v) for
752 intraperitoneal injection (100 μL/injection). The injections were administered on day
753 0, 3, 5, 7. DB doses corresponded to 1× (6.9 mg/kg) and 3× (20.7 mg/kg) molar
754 equivalents of Dox. All mice in the US groups received ultrasound irradiation (3 min,
755 procedures and acoustic parameters as previously described) at two time points (30
756 and 60 min post injection). Tumour volumes and body weights were measured daily.
757 Both Dox and Dox + US group had 3 mice sacrificed for exceeding 20% weight loss
758 on day 11 (n=3 on day 14). After 14 days treatment, the mice were euthanized.

759

760 Acute toxicity evaluation

761 The 4T1-tumour-bearing mice were randomized into four groups (n = 5): Ctrl
762 (PBS vehicle), Dox (30 mg/kg), DB (41.4 mg/kg), and DB + US (41.4 mg/kg + 2×3
763 min sonication 30/60 min post-injection), receiving intraperitoneal injections on days
764 0 and 2. Comprehensive toxicity profiling included daily weight monitoring, serum
765 biochemistry and organ coefficient analysis 24 h after the final dose.

766

767 In vivo antitumour evaluation of MMAE prodrug activation

768 When 4T1 tumour volume reached 40-100 mm^3, the tumour-bearing Balb/c mice
769 were randomly divided into five groups (n = 5): MMAE (0.5 mg/kg), MB (0.68
770 mg/kg), MB + US (0.68 mg/kg + 2 × 3 min sonication), US (PBS + 2 × 3 min
771 sonication) and PBS as control. MMAE (0.5 mg/kg) and MB (0.68 mg/kg, equivalent
772 to MMAE concentration of 0.5 mg/kg) were freshly formulated in PBS (5% DMSO,

v/v) for intravenous injection (100 μL/injection). The injections were administered intravenously on days 0, 5 and 10. All mice in the US groups received ultrasound irradiation (3 min, procedures and acoustic parameters as previously described) at two time points (30 and 60 min post injection). Tumour volumes and body weights were measured three times a week. After 21 days treatment, the mice were euthanized.

Long-term survival assessment

The 4T1-tumour-bearing mice were randomized into three groups (n = 10): PBS, MMAE (0.5 mg/kg), or MB+US (0.68 mg/kg). The injections were administered intravenously every 5 days (total 4 doses). Survival was monitored for 25 days with predefined humane endpoints. Kaplan-Meier curves were generated using event times (death or endpoint-triggered euthanasia).

In vivo antitumour evaluation of sono-caged BSA-MMAE conjugate activation

When 4T1 tumour volume reached 40-100 mm^3, the tumour-bearing Balb/c mice were randomly divided into three groups (n = 5): BSA-L1101 (47.2 mg/kg), BSA-L1101 + US (47.2 mg/kg + 3 × 5 min sonication), and PBS as control. BSA-L1101 (equivalent to MMAE concentration of 0.5 mg/kg) was formulated in PBS (5% DMSO, v/v) for intravenous injection (100 μL/injection). The injections were administered intravenously on days 0, 3 and 9. All mice in the US groups received ultrasound irradiation (5 min, procedures and acoustic parameters as previously described) at three time points (8, 24 and 48 h post injection). After 18 days treatment, the mice were euthanized.

Ethical statement

All animal procedures were approved by Peking University Institutional Animal Care and Use Committee (IACUC Approval # DLASBE0714, DLASBE0716) and conducted in strict accordance with institutional ethical guidelines. During our research, any mouse with tumour volume exceeding 1,200 mm^3 or weight loss exceeding 20% of the normal weight was euthanized. At the end of the experiment, all

the mice were immediately euthanized.

Statistics

Data are expressed as the mean ± standard deviation (s.d.) or standard error of the mean (s.e.m.) as indicated in each of the figure legend. Statistical significance was determined using a two-tailed unpaired Student's *t*-test when only two value sets were compared or by ANOVA for comparison between multiple groups via Prism 9.5. Exact *P* values are documented in the figures or figure legends. Difference was considered to be significant if $P < 0.05$, ($*P < 0.05$, $**P < 0.01$, $***P < 0.001$, $****P < 0.0001$ unless otherwise indicated).

Acknowledgement

G.L. is supported by the National Natural Science Foundation of China (22377005), and the Beijing Natural Science Foundation (JQ22021).

References

1 Wang, X., Wang, X., Jin, S., Muhammad, N. & Guo, Z. Stimuli-Responsive Therapeutic Metallodrugs. *Chem Rev* **119**, 1138-1192, doi:10.1021/acs.chemrev.8b00209 (2019).

2 Xu, W. *et al.* Stimuli-responsive prodrugs with self-immolative linker for improved cancer therapy. *Eur J Med Chem* **279**, 116928, doi:10.1016/j.ejmech.2024.116928 (2024).

3 Wei, D., Sun, Y., Zhu, H. & Fu, Q. Stimuli-Responsive Polymer-Based Nanosystems for Cancer Theranostics. *ACS Nano* **17**, 23223-23261, doi:10.1021/acsnano.3c06019 (2023).

4 Gorrini, C., Harris, I. S. & Mak, T. W. Modulation of oxidative stress as an anticancer strategy. *Nat Rev Drug Discov* **12**, 931-947, doi:10.1038/nrd4002 (2013).

5 Sies, H. & Jones, D. P. Reactive oxygen species (ROS) as pleiotropic physiological signalling agents. *Nat Rev Mol Cell Biol* **21**, 363-383, doi:10.1038/s41580-020-0230-3 (2020).

6 Winterbourn, C. C. Reconciling the chemistry and biology of reactive oxygen species. *Nat Chem Biol* **4**, 278-286, doi:10.1038/nchembio.85 (2008).

7 Dickinson, B. C. & Chang, C. J. Chemistry and biology of reactive oxygen species in signaling or stress responses. *Nat Chem Biol* **7**, 504-511, doi:10.1038/nchembio.607 (2011).

8 Lippert, A. R., Van de Bittner, G. C. & Chang, C. J. Boronate oxidation as a bioorthogonal reaction approach for studying the chemistry of hydrogen peroxide in living systems. *Acc Chem Res* **44**, 793-804, doi:10.1021/ar200126t (2011).

9 Saravanakumar, G., Kim, J. & Kim, W. J. Reactive-Oxygen-Species-Responsive Drug Delivery Systems: Promises and Challenges. *Adv Sci (Weinh)* **4**, 1600124, doi:10.1002/advs.201600124

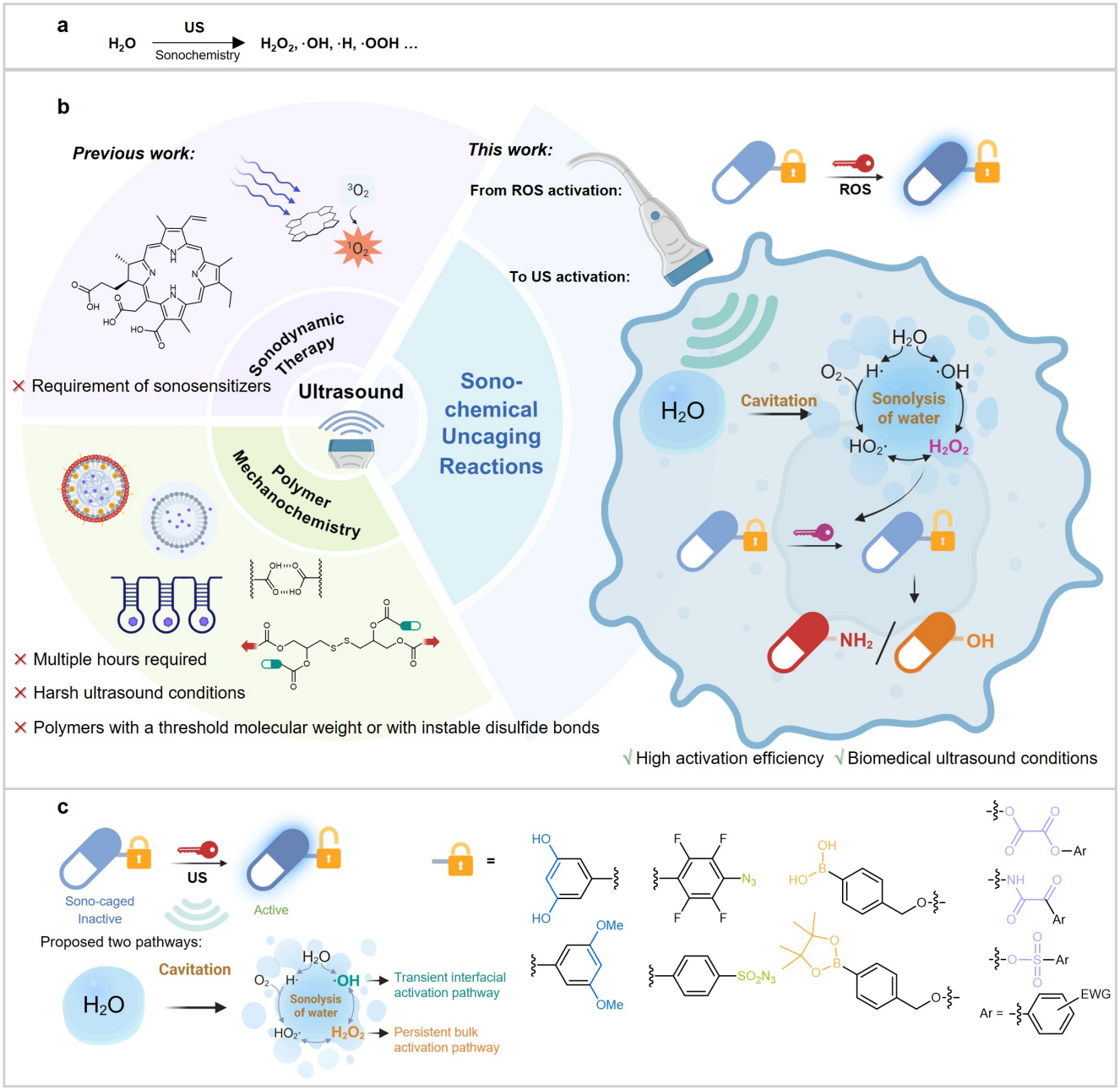
(2017).
10 Wang, L. *et al.* Exogenous/endogenous stimuli-responsive antitumor prodrugs advance precision chemotherapy. *Bioorg Med Chem* **132**, 118485, doi:10.1016/j.bmc.2025.118485 (2026).
11 Gong, Z. & Dai, Z. Design and Challenges of Sonodynamic Therapy System for Cancer Theranostics: From Equipment to Sensitizers. *Adv Sci (Weinh)* **8**, 2002178, doi:10.1002/advs.202002178 (2021).
12 Fu, X. & Hu, X. Ultrasound-Controlled Prodrug Activation: Emerging Strategies in Polymer Mechanochemistry and Sonodynamic Therapy. *ACS Appl Bio Mater* **7**, 8040-8058, doi:10.1021/acsabm.4c00150 (2024).
13 Ren, X., Zhang, H., Zhang, J., Shen, N. & Tang, Z. Ultrasound-Activated Prodrugs for Precision Cancer Therapy: From Mechanical and Cavitation Effects to Advanced Sonochemical Activation. *Chem & Bio Engineering* (2026).
14 Zuo, M. *et al.* Ultrasound-activated mechanochemical reactions for controllable biomedical applications. *Smart Materials in Medicine* **5**, 461-476, doi:https://doi.org/10.1016/j.smaim.2024.09.001 (2024).
15 Huo, S. *et al.* Mechanochemical bond scission for the activation of drugs. *Nat Chem* **13**, 131-139, doi:10.1038/s41557-020-00624-8 (2021).
16 Shi, Z., Wu, J., Song, Q., Göstl, R. & Herrmann, A. Toward Drug Release Using Polymer Mechanochemical Disulfide Scission. *J Am Chem Soc* **142**, 14725-14732, doi:10.1021/jacs.0c07077 (2020).
17 Shi, Z., Song, Q., Göstl, R. & Herrmann, A. Mechanochemical activation of disulfide-based multifunctional polymers for theranostic drug release. *Chem Sci* **12**, 1668-1674, doi:10.1039/d0sc06054b (2020).
18 Wang, W. *et al.* H-bonded organic frameworks as ultrasound-programmable delivery platform. *Nature* **638**, 401-410, doi:10.1038/s41586-024-08401-0 (2025).
19 Huo, S. *et al.* Mechano-Nanoswitches for Ultrasound-Controlled Drug Activation. *Adv Sci (Weinh)* **9**, e2104696, doi:10.1002/advs.202104696 (2022).
20 Sirsi, S. R. & Borden, M. A. State-of-the-art materials for ultrasound-triggered drug delivery. *Adv Drug Deliv Rev* **72**, 3-14, doi:10.1016/j.addr.2013.12.010 (2014).
21 Tong, Y. *et al.* Urea-Bond Scission Induced by Therapeutic Ultrasound for Biofunctional Molecule Release. *J Am Chem Soc* **144**, 16799-16807, doi:10.1021/jacs.2c03669 (2022).
22 Liu, G. *et al.* An ultrasound-activatable platinum prodrug for sono-sensitized chemotherapy. *Sci Adv* **9**, eadg5964, doi:10.1126/sciadv.adg5964 (2023).
23 Yang, Z. *et al.* Programmable Bacterial Architects Crafting Sonosensitizers for Tumor-Specific Sonodynamic Immunotherapy. *Adv Mater* **37**, e2504206, doi:10.1002/adma.202504206 (2025).
24 He, F. *et al.* Progress of Piezoelectric Semiconductor Nanomaterials in Sonodynamic Cancer Therapy. *ACS Biomater Sci Eng* **10**, 298-312, doi:10.1021/acsbiomaterials.3c01232 (2024).
25 Yao, Y. *et al.* Remote control of mechanochemical reactions under physiological conditions using biocompatible focused ultrasound. *Proc Natl Acad Sci U S A* **120**, e2309822120, doi:10.1073/pnas.2309822120 (2023).
26 Huang, H. *et al.* Ultrasound-Based Micro-/Nanosystems for Biomedical Applications. *Chem Rev* **124**, 8307-8472, doi:10.1021/acs.chemrev.4c00009 (2024).

27 Li, T. *et al.* An ultrasound-activated PROTAC prodrug with self-reporting fluorescence for targeted protein degradation. *Biomaterials* **330**, 124045, doi:10.1016/j.biomaterials.2026.124045 (2026).
28 Chen, F. *et al.* Polypeptide sono-adjuvant for ultrasound-activatable regulation of innate immunity and cancer vaccination therapy. *Nat Commun* **17**, 272, doi:10.1038/s41467-025-66976-2 (2025).
29 Tan, W. *et al.* Ultrasound-Activated Prodrugs for Tumor-Specific Immunotherapy. *J Am Chem Soc* **148**, 11296-11308, doi:10.1021/jacs.6c00735 (2026).
30 Fu, X. *et al.* Ultrasound-triggered prodrug activation via sonochemically induced cleavage of a 3,5-dihydroxybenzyl carbamate scaffold. *Chem Sci* **16**, 21000-21009, doi:10.1039/d5sc05710h (2025).
31 Luo, C., Kong, C., Zhang, Y., Xu, Y. & Tang, Z. Ultrasound-responsive azide nano-prodrugs enable spatiotemporal activation of TLR7/8 agonists for tumor therapy. *Biomater Sci* **13**, 5390-5401, doi:10.1039/d5bm00755k (2025).
32 Xu, H. *et al.* Ultrasound-Triggered Activation of p-Azidobenzyloxycarbonyl-Based Prodrugs via Radical-Mediated Cascade Elimination. *J Am Chem Soc* **147**, 20667-20679, doi:10.1021/jacs.5c03878 (2025).
33 Qin, S. *et al.* Remote Molecule Activation in Living Mice Triggered by Therapeutic Ultrasound. *Angew Chem Int Ed Engl* **65**, e25894, doi:10.1002/anie.202525894 (2026).
34 Manickam, S. *et al.* Ultrasonics and sonochemistry: Editors' perspective. *Ultrason Sonochem* **99**, 106540, doi:10.1016/j.ultsonch.2023.106540 (2023).
35 Meng, T. *et al.* Introduction of the α-ketoamide structure: en route to develop hydrogen peroxide responsive prodrugs. *Chem Sci* **10**, 7156-7162, doi:10.1039/c9sc00910h (2019).
36 Maeda, H. *et al.* Fluorescent probes for hydrogen peroxide based on a non-oxidative mechanism. *Angew Chem Int Ed Engl* **43**, 2389-2391, doi:10.1002/anie.200452381 (2004).
37 Geng, J. *et al.* Switching on prodrugs using radiotherapy. *Nat Chem* **13**, 805-810, doi:10.1038/s41557-021-00711-4 (2021).
38 Yang, C., Yang, Y., Li, Y., Ni, Q. & Li, J. Radiotherapy-Triggered Proteolysis Targeting Chimera Prodrug Activation in Tumors. *J Am Chem Soc* **145**, 385-391, doi:10.1021/jacs.2c10177 (2023).
39 Fu, Q. *et al.* External-Radiation-Induced Local Hydroxylation Enables Remote Release of Functional Molecules in Tumors. *Angew Chem Int Ed Engl* **59**, 21546-21552, doi:10.1002/anie.202005612 (2020).
40 Wang, C., Zhang, Z. & Liu, Z. Radiotherapy-Activated Prodrug: Past, Present and Beyond. *ACS Cent Sci* **11**, 1306-1320, doi:10.1021/acscentsci.5c00875 (2025).
41 Peng, K., Qin, F. G. F., Jiang, R., Qu, W. & Wang, Q. Production and dispersion of free radicals from transient cavitation Bubbles: An integrated numerical scheme and applications. *Ultrason Sonochem* **88**, 106067, doi:10.1016/j.ultsonch.2022.106067 (2022).
42 Peng, K., Tian, S., Zhang, Y., He, Q. & Wang, Q. Penetration of hydroxyl radicals in the aqueous phase surrounding a cavitation bubble. *Ultrason Sonochem* **91**, 106235, doi:10.1016/j.ultsonch.2022.106235 (2022).
43 Murphy, M. P. *et al.* Guidelines for measuring reactive oxygen species and oxidative damage in cells and in vivo. *Nat Metab* **4**, 651-662, doi:10.1038/s42255-022-00591-z (2022).
44 Wang, L. *et al.* Overlooked Formation of H(2)O(2) during the Hydroxyl Radical-Scavenging

Process When Using Alcohols as Scavengers. *Environ Sci Technol* **56**, 3386-3396, doi:10.1021/acs.est.1c03796 (2022).

45 Hingorani, D. V. *et al.* Monomethyl auristatin antibody and peptide drug conjugates for trimodal cancer chemo-radio-immunotherapy. *Nat Commun* **13**, 3869, doi:10.1038/s41467-022-31601-z (2022).

46 Fontmorin, J. M., Burgos Castillo, R. C., Tang, W. Z. & Sillanpää, M. Stability of 5,5-dimethyl-1-pyrroline-N-oxide as a spin-trap for quantification of hydroxyl radicals in processes based on Fenton reaction. *Water Res* **99**, 24-32, doi:10.1016/j.watres.2016.04.053 (2016).



938 **Fig. 1 | Conceptual framework of ultrasound-triggered molecular activation. a**, Schematic
939 depiction of reactive oxygen species generation from water under ultrasound irradiation. **b**, The
940 conceptual advance from previous ultrasound activation modes to sonochemical uncaging reactions
941 based on water sonolysis. **c**, Masking-group screening and the proposed activation model for boronate
942 uncaging. Representative ROS-responsive functional groups were evaluated for ultrasound-triggered
943 uncaging. Two sonochemical activation behaviours were considered to guide productive trigger
944 selection.
945
946

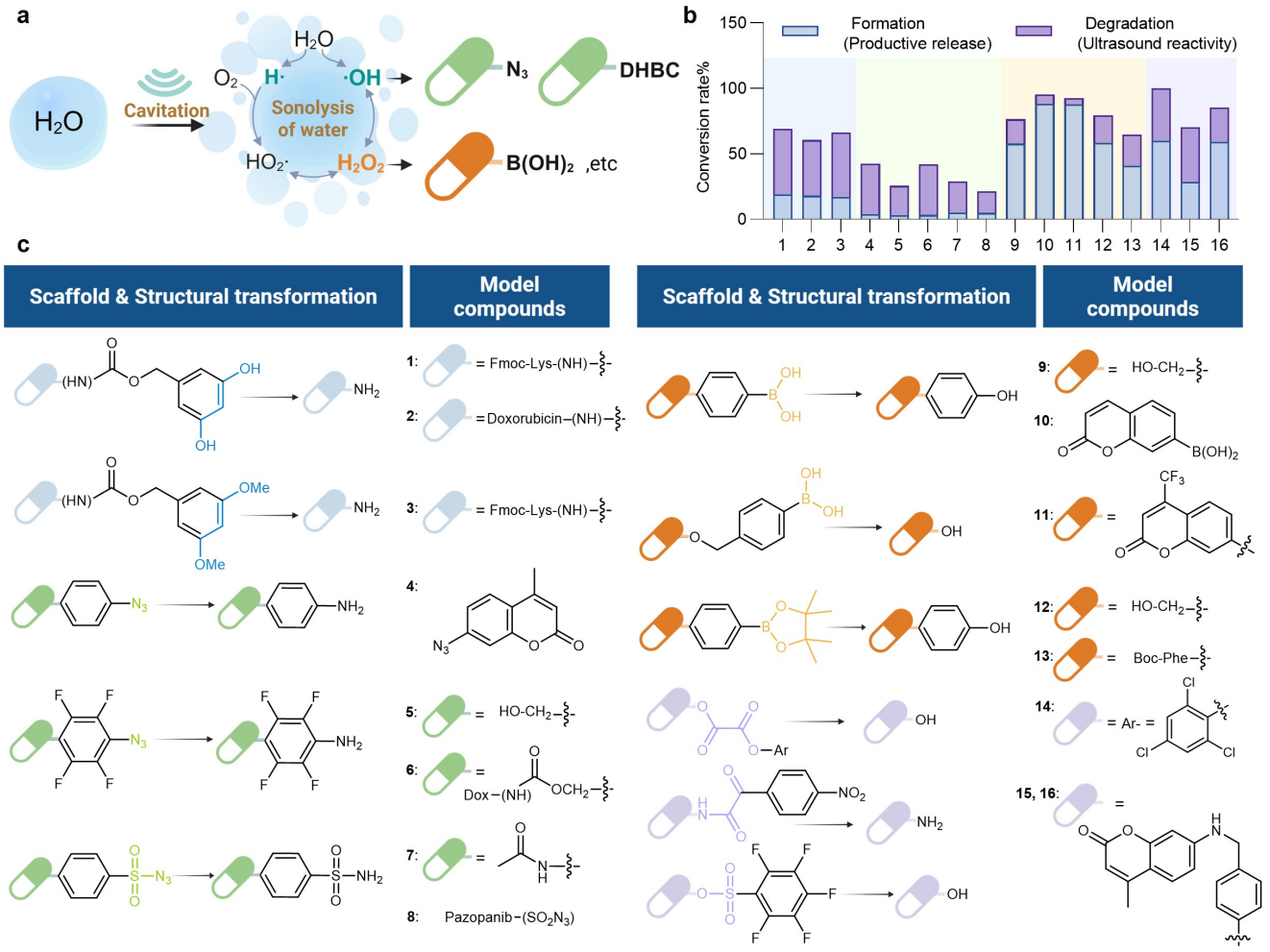


Fig. 2 | Representative screening of ROS-responsive masking groups under ultrasound irradiation. a, Schematic illustration of the rationale for functional-group screening under ultrasound. Ultrasound-induced cavitation and sonolysis of water generate multiple reactive oxygen species, which may activate structurally distinct ROS-responsive masking groups. **b**, Quantitative summary of ultrasound-induced product distribution for representative substrates. The relative proportions of desired product formation and undesired degradation were determined after ultrasound treatment under a common screening condition (1 MHz, 3.0 W/cm^2, 70% duty cycle, 3 min). Compounds **1**–**16** correspond to the representative substrates shown in panel c. **c**, Schematic overview of representative masking-group scaffolds, expected structural transformations, and screening substrates. Among the tested substrates, boronic acid/boronate groups showed the most favorable balance between productive release and limited degradation, and were therefore selected for further mechanistic and biological investigation.

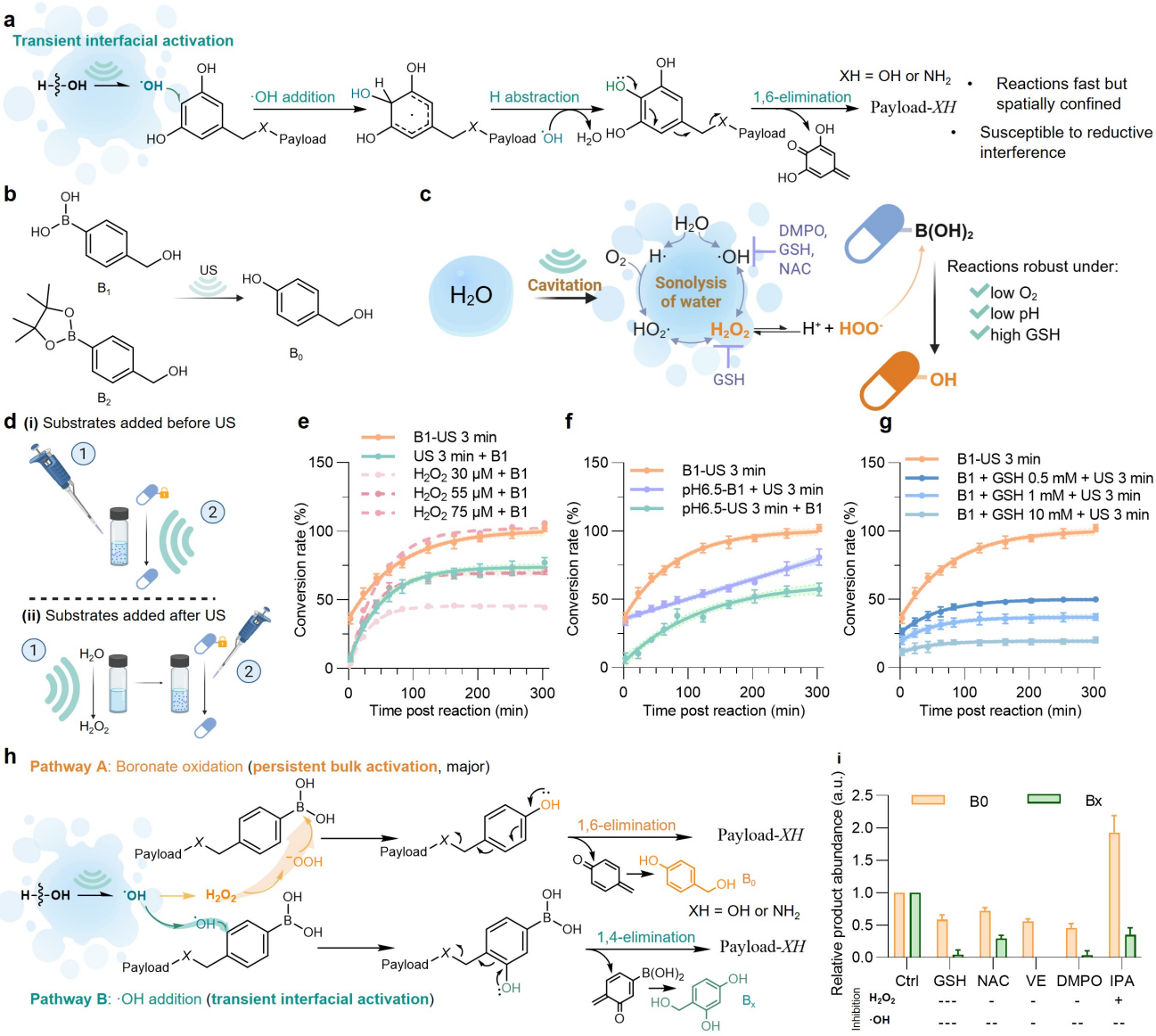


Fig. 3 | Comparative mechanistic dissection of transient interfacial activation and persistent bulk activation of representative motifs under ultrasound irradiation. **a**, Schematic illustration of the proposed transient interfacial activation mode for DHBC-type masking groups. **b**, Schemes of boronic acid-caged model compounds uncaging under ultrasound irradiation (1 MHz, 3.0 W/cm^2, 70% duty cycle, 3 min). **c**, Schematic summary of the operative ROS environment and the robustness of ultrasound-triggered boronic acid activation. Both hydrogen peroxide and short-lived radical species are generated under ultrasound, and productive uncaging is maintained under tumour-mimicking conditions, including low oxygen tension, mildly acidic pH, and elevated glutathione. **d**, Schematic illustration of direct versus delayed substrate exposure experiments. Comparison of substrates irradiated directly under ultrasound (substrate + US) with those added after ultrasound pretreatment (US + substrate) distinguishes persistent ROS-mediated activation from contributions requiring transient reactive intermediates. **e–g**, Kinetic analyses of boronic acid uncaging of B1 (10 μM in 0.02 M PBS buffer, under aforesaid US condition) to B0 under different reaction conditions (**e**, comparison with exogenous H_2O_2; **f**, mildly acidic pH; **g**, increasing GSH concentrations; $n = 3$, mean ± s.d.). **h**, Schematic illustration of the proposed dual-pathway mechanism for boronic acid activation under ultrasound. A peroxide-enabled boronate oxidation pathway is proposed as the major productive route,

977 whereas hydroxyl radical-assisted aromatic addition constitutes a possible parallel pathway under
978 ultrasound. **i**, Product-distribution analysis supporting mechanistic divergence between bulk
979 peroxide-driven release and interfacial radical-associated side chemistry. The relative abundances of
980 characteristic products (B0) and byproducts (Bx) under different conditions (scavengers 1 mM) are
981 displayed.
982
983

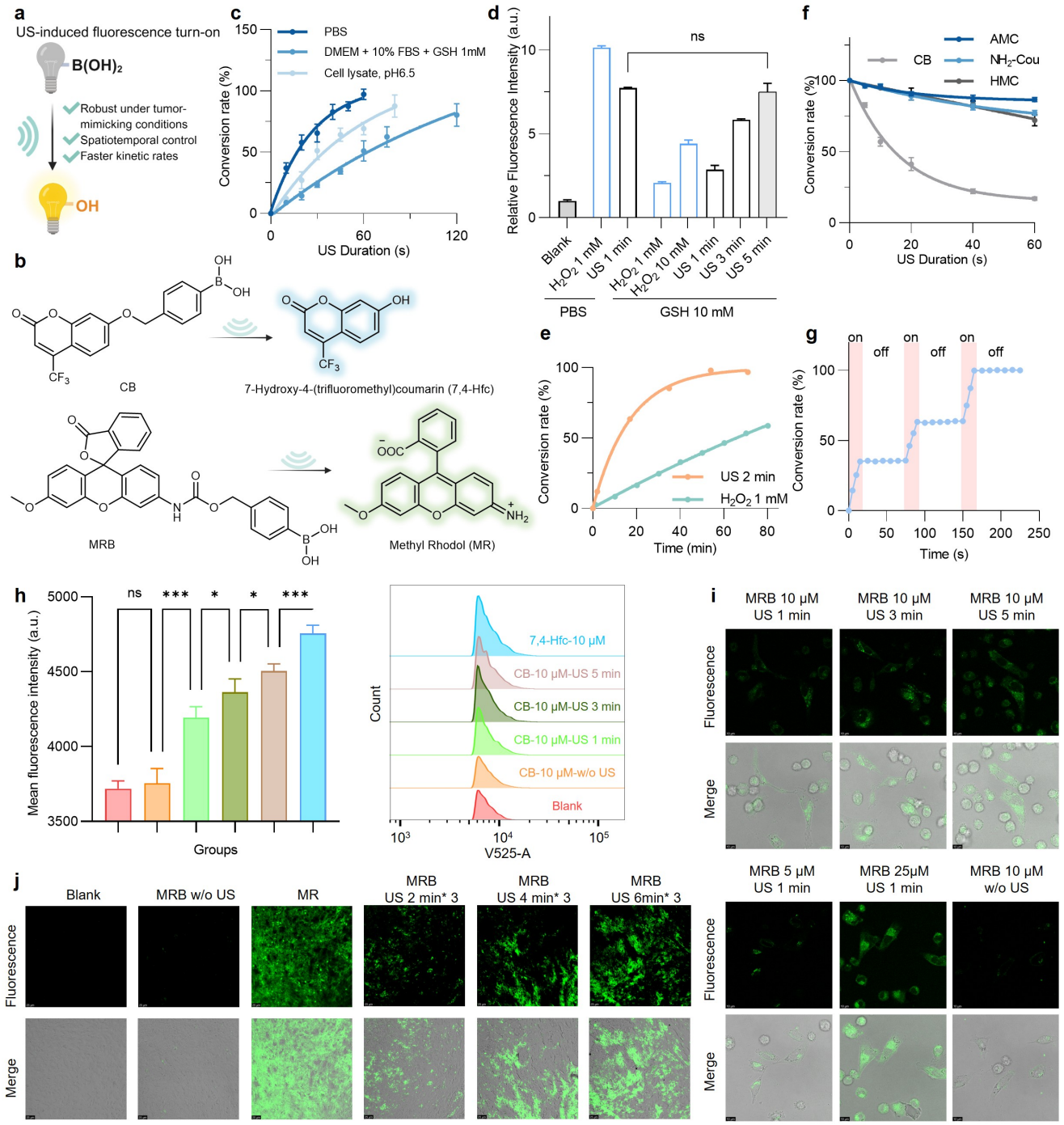


Fig.4 | Ultrasound-triggered boronic acid/boronate-caged functional probe activation in biologically relevant environments and living systems. a, Schematic depiction of the advantages of ultrasound-triggered fluorogenic activation. **b**, Schemes of boronic acid-caged probes uncaging under ultrasound irradiation (1 MHz, 3.0 W/cm^2, 70% duty cycle, 3 min). **c**, Conversion kinetics of CB (10 μM) under ultrasound irradiation in complex environments (PBS; DMEM + 10% FBS + GSH 1mM; cell lysate, pH 6.5). **d**, Endpoint fluorescence summary comparing ultrasound-triggered and H_2O_2-triggered CB (10 μM) activation in PBS and under reductive conditions (10 mM GSH). **e**, Kinetic comparison of ultrasound-triggered and exogenous H_2O_2-triggered fluorogenic activation of MRB (10 μM). **f**, Competitive selectivity analysis of ultrasound-triggered CB (10 μM in PBS) activation in the presence of structurally related unprotected coumarins. **g**, Temporal-programming analysis of

ultrasound-triggered compound **10** (100 μM in PBS) activation by repeated on/off US irradiation cycles. **h**, Flow cytometry analysis (V525-A) of MDA-MB-231 cells incubated with CB (10 μM), with 7,4-Hfc generated in cells following US irradiation for 1 min, 3 min and 5 min (1.0 W/cm^2, 10% duty cycle). Flow cytometry analyses are based on a population of 5,000 cells (n = 5). Statistical significance was determined as $P > 0.05$ (ns), $P < 0.05$ (*), $P < 0.01$ (**), $P < 0.001$ (***) by a Tukey's test. The histogram indicating the percentage of 7,4-Hfc-positive cells in flow cytometry. **i**, Representative confocal fluorescence images of MDA-MB-231 cells after being treated with increased irradiation duration or increased MRB concentrations. Scale bar, 10 μm. Three independent experiments were performed and the representative results are shown. **j**, Representative confocal fluorescence images of tumour sections. Scale bar, 25 μm. Balb/c mice implanted subcutaneously with 4T1 cells were used (n = 3 mice per group). The experimental groups of mice were given MRB (0.6 mg/kg) and then received ultrasound irradiation (2.5 W/cm^2, 70% duty cycle) for three separate times for indicated durations.

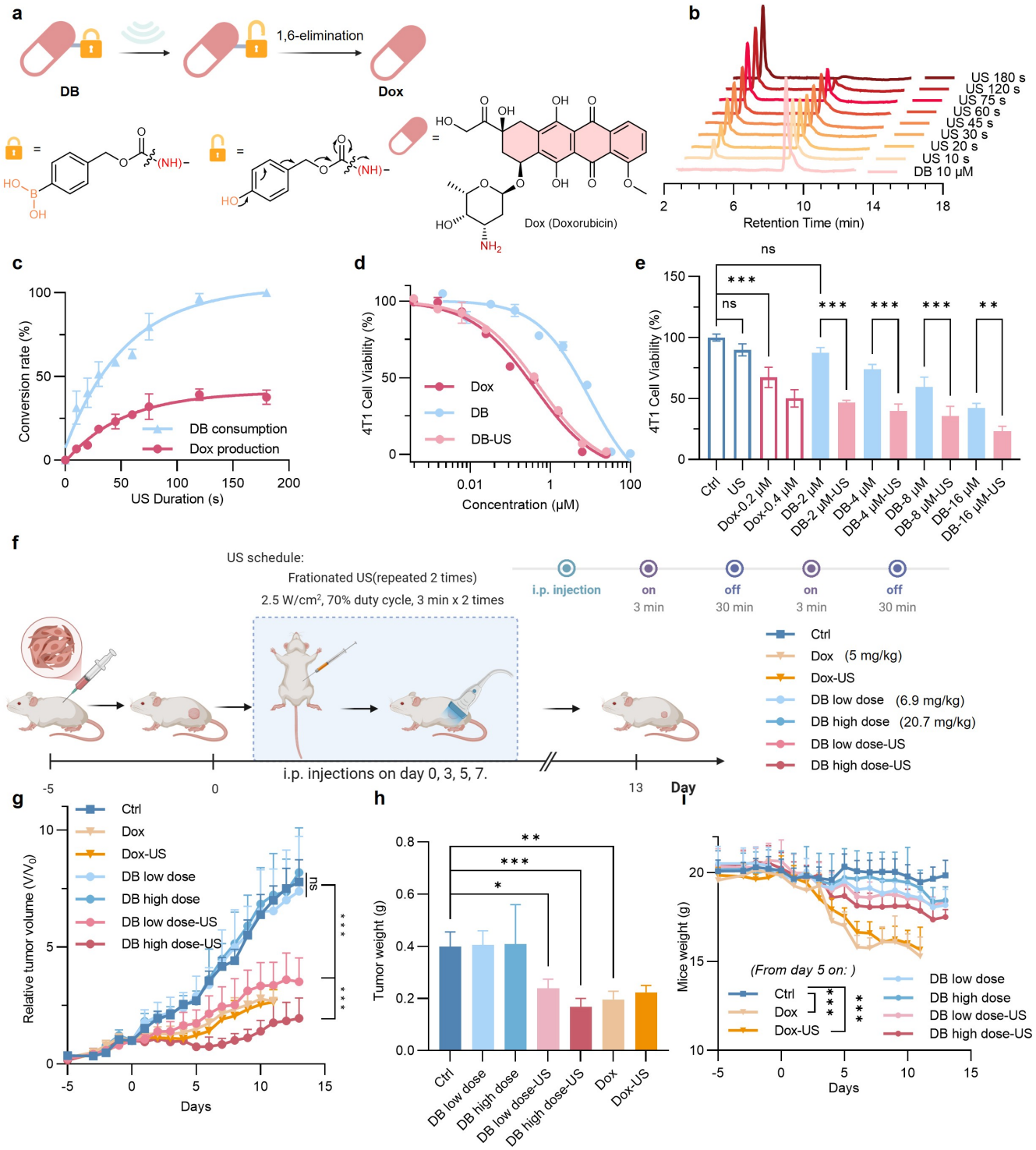
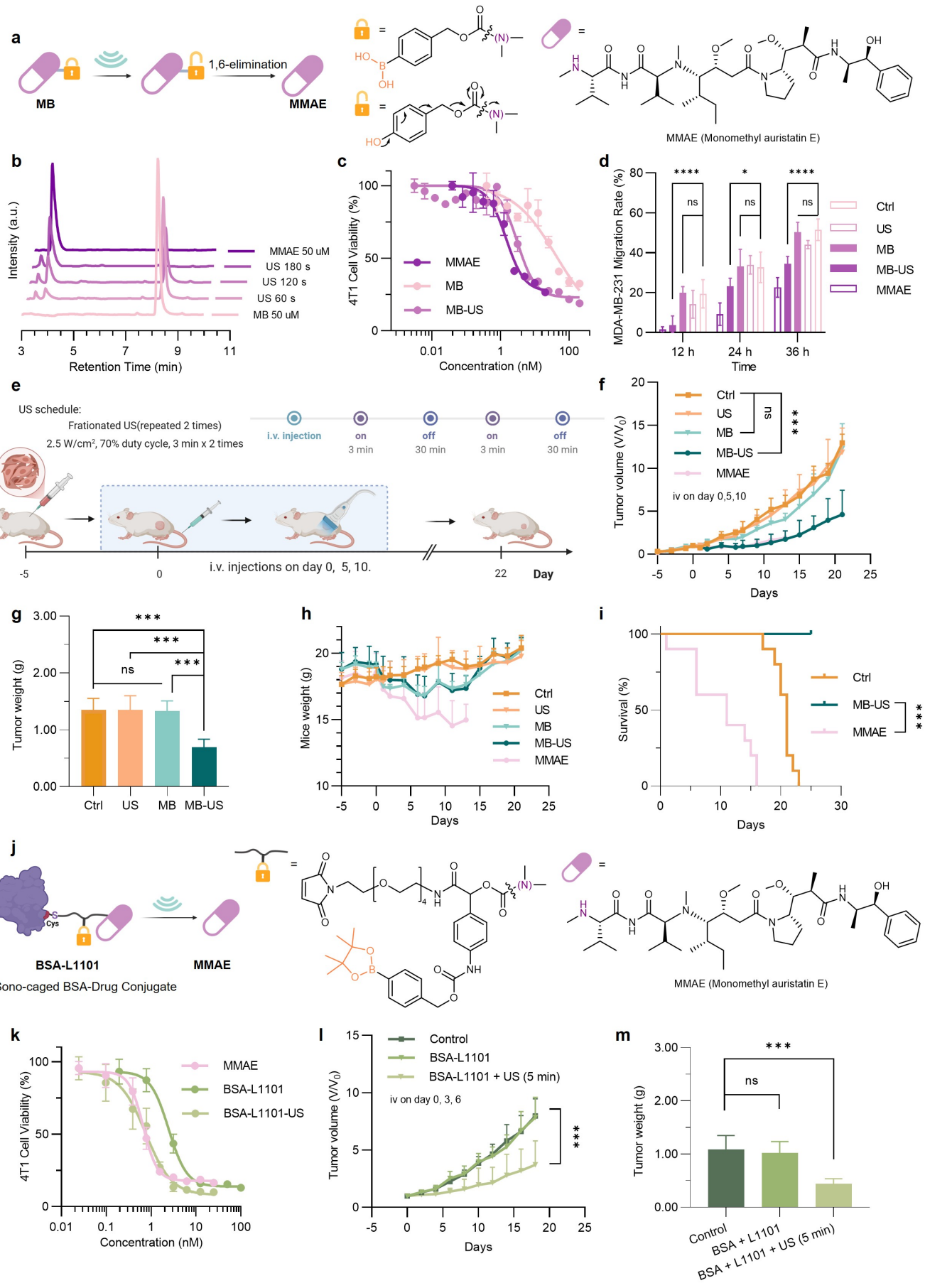


Fig.5 | Ultrasound-triggered activation of a boronic acid/boronate-caged doxorubicin prodrug. a, US irradiation triggers the doxorubicin prodrug DB activation and releases Dox. **b**, HPLC traces for the reaction mixture of prodrug DB after US irradiation with increasing duration, showing unreacted prodrug DB (R_T = 8.80 min) and doxorubicin (R_T = 4.67 min). **c**, The conversion rate of DB (10 μM in 0.02 M PBS buffer) into Dox under US irradiation (1 MHz, 3.0 W/cm^2, 70% duty cycle). **d**, Cell viability curve (4T1 cells) of US-induced doxorubicin prodrug activation in vitro. The prodrug was irradiated under ex situ ultrasound (3.0 W/cm^2, 70% duty cycle, 3 min). **e**, Cell viability assay (4T1 cells) of US-induced doxorubicin prodrug activation in situ. The prodrug was irradiated under cell-friendly ultrasound (1.0

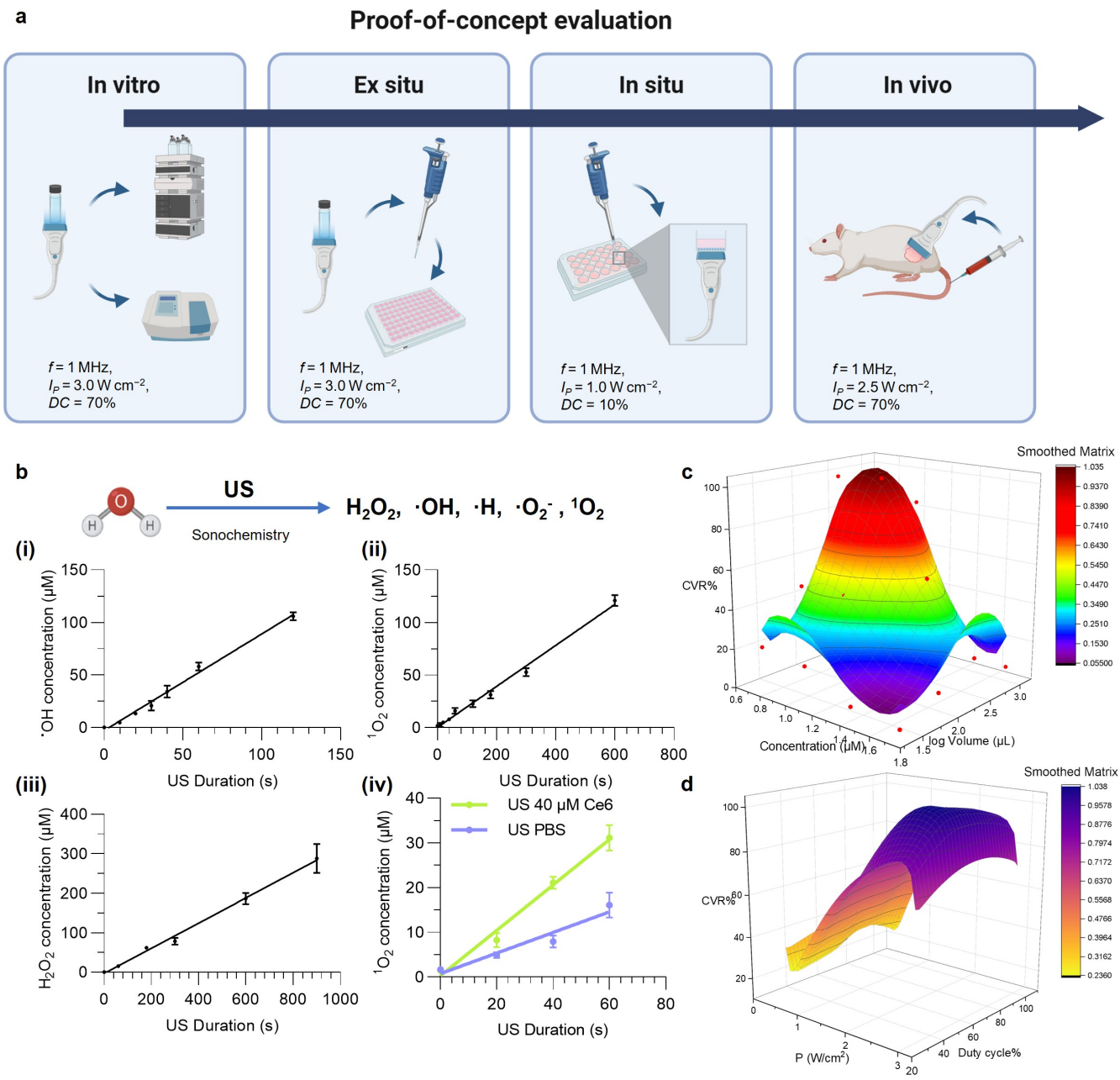
W/cm^2, 10% duty cycle, 5 min). Cell viability was measured using an MTT assay after 48 h of incubation at 37 °C. **f**, Schematic illustration of intraperitoneal administration of prodrug DB and US irradiation in the 4T1 tumour-bearing Balb/c mice model. **g**, Tumour growth curves of different groups after various treatments. Mice in the Ctrl group received intraperitoneal injection of PBS (100 μL). Dox group received intraperitoneal injection of Dox (5 mg/kg). DB low dose group received intraperitoneal injection of DB (6.9 mg/kg) and high dose group received DB (20.7 mg/kg). All mice in the US groups received ultrasound irradiation (2.5 W/cm^2, 70% duty cycle, 3 min) for two separate times (30 min and 60 min post injection). Tumour burdens were measured every other day using a caliper. The data are presented as mean ± s.d. (n = 6). Statistical analysis was performed using one-way ANOVA with Dunnett post-test compared to PBS-treated mice. **h**, Average weights of excised 4T1 tumours on day 14 (n = 6 except for Dox group and Dox-US group). Both Dox and Dox-US group had 3 mice sacrificed for exceeding the ethical weight limit on day 11 (n = 3 on day 14). **i**, Weight change curves of mice (n = 6 mice per group, mean ± s.d.). Statistical significance was determined as $P > 0.05$ (ns), $P < 0.05$ (*), $P < 0.01$ (**), $P < 0.001$ (***) by a Tukey's test.



1031 **Fig.6 | Ultrasound-triggered activation of boronic acid/boronate-caged MMAE prodrugs and an**

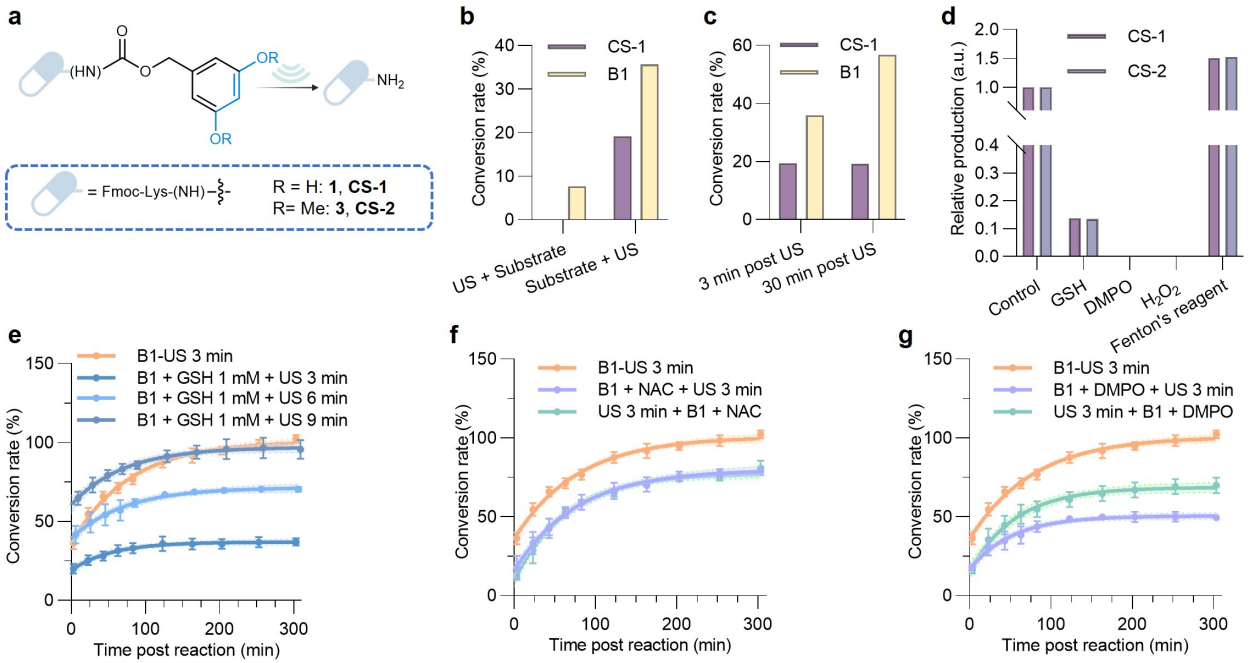
albumin–MMAE conjugate. a, US irradiation triggers the release of potent cytotoxic drug MMAE. **b**, HPLC traces for the reaction mixture of prodrug MB (50 μM in 0.02 M PBS buffer) after US irradiation with increasing duration, showing unreacted prodrug MB (R_T = 7.67 min) and MMAE (R_T = 3.87 min). **c**, Cell viability test (4T1 cells) of US-induced MMAE prodrug activation in vitro. The prodrug MB was irradiated under ex situ ultrasound (3.0 W/cm^2, 70% duty cycle, 3 min). **d**, Scratch assay of MDA-MB-231 cells after 12 h of treatment with different conditions (Ctrl, US, MMAE, MB and MB-US). The prodrug MB was irradiated under in situ ultrasound (1.0 W/cm^2, 10% duty cycle, 5 min). The images show the migration of cells into the scratched area at different time points. **e**, Schematic illustration of intravenous administration of prodrug MB and US irradiation in the 4T1 tumour-bearing Balb/c mice model. **f**, Tumour growth curves of different groups after various treatments. Mice in the Ctrl and US groups received intravenous injection of PBS (100 μL). MMAE group received intravenous injection of MMAE (0.5 mg/kg). MB group received intravenous injection of MB (0.5 mg/kg). The injections were administered on day 0, 5, 10. Mice in the US and MB-US groups received ultrasound irradiation (2.5 W/cm^2, 70% duty cycle, 3 min) for two separate times (30 min and 60 min post injection). Tumour burdens were measured every other day using a caliper. The data are presented as mean ± s.d. (n = 5). Statistical analysis was performed using one-way ANOVA with Dunnett post-test compared to PBS-treated mice. Mice in MMAE group exceeding the ethical weight limit were executed on the same day. **g**, Average weights of excised 4T1 tumours on day 14 (n = 5). **h**, Weight change curves of mice (n = 5 mice per group, mean ± s.d.). **i**, Kaplan-Meier survival analysis of mice in different treatment groups. Mice in groups of Ctrl, MB-US, and MMAE (n = 10 mice per group. The dose administered was the same as above, and the frequency of administration was twice a week.) were monitored for survival over 25 days. Mice were sacrificed when endpoint criteria were met. The log-rank test was used to assess statistical significance between groups (P < 0.0001). **j**, Design of sono-caged BSA-MMAE conjugate (BSA-L1101) and its conversion under US to free drug MMAE. **k**, Cell viability test (4T1 cells) of US-induced BSA-L1101 conjugate activation in vitro. **l**, Tumour growth curves after intravenous administration of the conjugate prodrug BSA-L1101 and US irradiation in the 4T1 tumour-bearing Balb/c nude mice model. **m**, Average weights of excised 4T1 tumours on day 14 (n = 5). Statistical significance was determined as P > 0.05 (ns), P < 0.05 (*), P < 0.01 (**), P < 0.001 (***) by a Tukey's test.

Extended Figures:

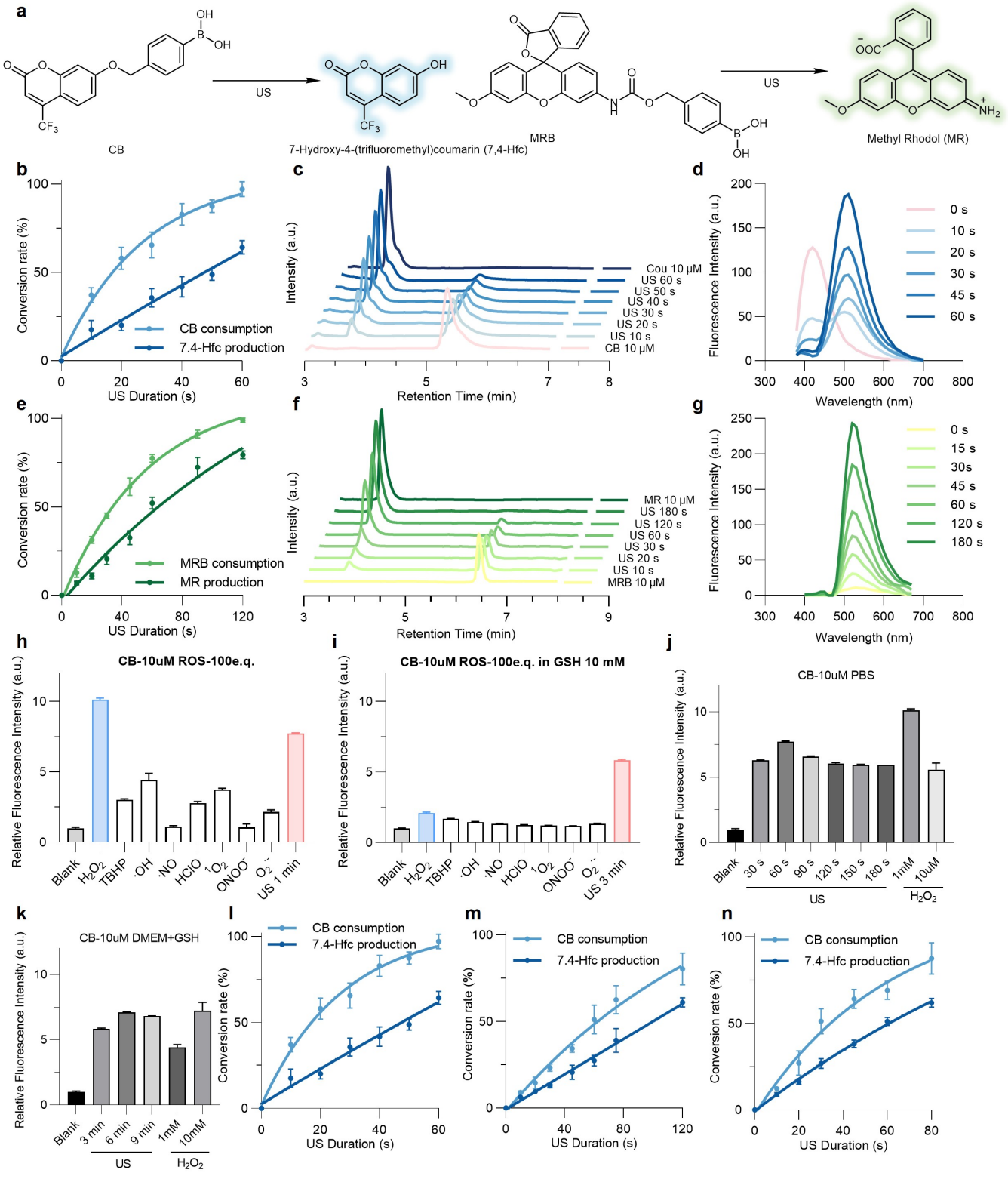


Extended Data Fig. 1 | Experimental workflow, ROS generation under ultrasound, and optimization of ultrasound-triggered conversion conditions. a, Schematic illustration of the overall experimental workflow from local proof-of-concept activation to systemically administered therapeutic validation. The study design progresses from ultrasound-triggered activation chemistry and masking-group screening to mechanistic dissection, fluorogenic probe validation, and in vivo prodrug therapy. **b**, Time-dependent generation of major reactive oxygen species during ultrasound irradiation. (**i-iii**), Representative measurements show ultrasound-induced production of hydroxyl radicals, singlet oxygen, and hydrogen peroxide as a function of irradiation time, establishing a composite ROS environment generated from cavitation-driven water sonolysis. **(iv)**, Comparison of singlet oxygen generation by direct ultrasound irradiation and conventional sonodynamic treatment. Ultrasound alone generates a relatively lower but still significant concentration of singlet oxygen than Ce6-mediated

sonodynamic treatment, supporting the distinct mechanistic basis of the present sonochemical activation mode. **c**, Effects of sample concentration and reaction volume on ultrasound-triggered conversion. The conversion efficiency depends on substrate concentration and irradiation volume, reflecting the relationship between ROS generation, cavitation conditions, and productive uncaging. **d**, Effects of ultrasound power and duty cycle on conversion efficiency. Ultrasound-triggered activation exhibits clear parameter dependence, and productive uncaging increases with irradiation intensity once the cavitation threshold is exceeded.

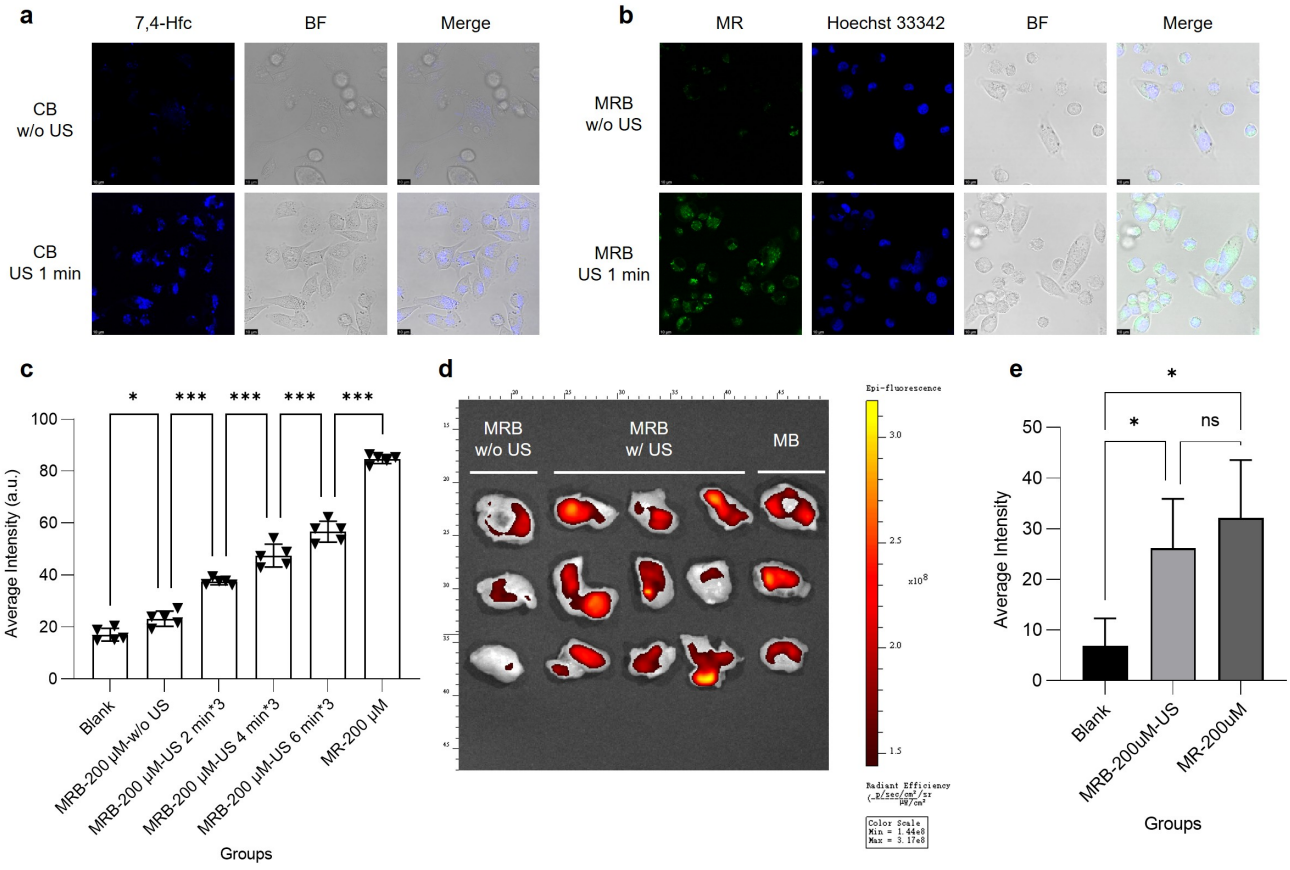


Extended Data Fig. 2 | Additional mechanistic analyses of DHBC and boronic acid activation under ultrasound irradiation. **a**, Schematic illustration of ultrasound-triggered activation of DHBC/DMOBC-caged substrates. **b,** Comparison of direct substrate ultrasound irradiation and delayed addition for DHBC- and boronic-acid-caged substrates. **c**, Comparison of immediate (within 3 min) and 30 min post-sonication conversion for DHBC- and boronic-acid-caged substrates. **d**, Ultrasound-triggered conversion of DHBC-caged model substrates CS-1 and CS-2 under different reaction conditions (Ctrl: US 3 min; GSH: 1 mM; DMPO: 1 mM; H_2O_2: 1 mM; Fenton's reagent: H_2O_2 10 mM and Fe (II) 1 mM). In vivo tumour-growth analyses compare the therapeutic consequences of two distinct masking-group chemistries under otherwise similar ultrasound-triggered treatment conditions (2.5 W/cm^2, 70% duty cycle, 3 min). **e,** Effect of 1 mM GSH and recovery of activation by prolonged ultrasound exposure. **f–g**, Effects of selected additives on ultrasound-triggered boronic acid uncaging. Conversion of B1 was evaluated under direct ultrasound exposure, co-incubation with additives during ultrasound, or addition after ultrasound pretreatment of the medium. These experiments distinguish persistent bulk oxidant-mediated activation from contributions requiring transient reactive intermediates. **f,** Effect of 1 mM NAC. **g,** Effect of 1 mM DMPO.

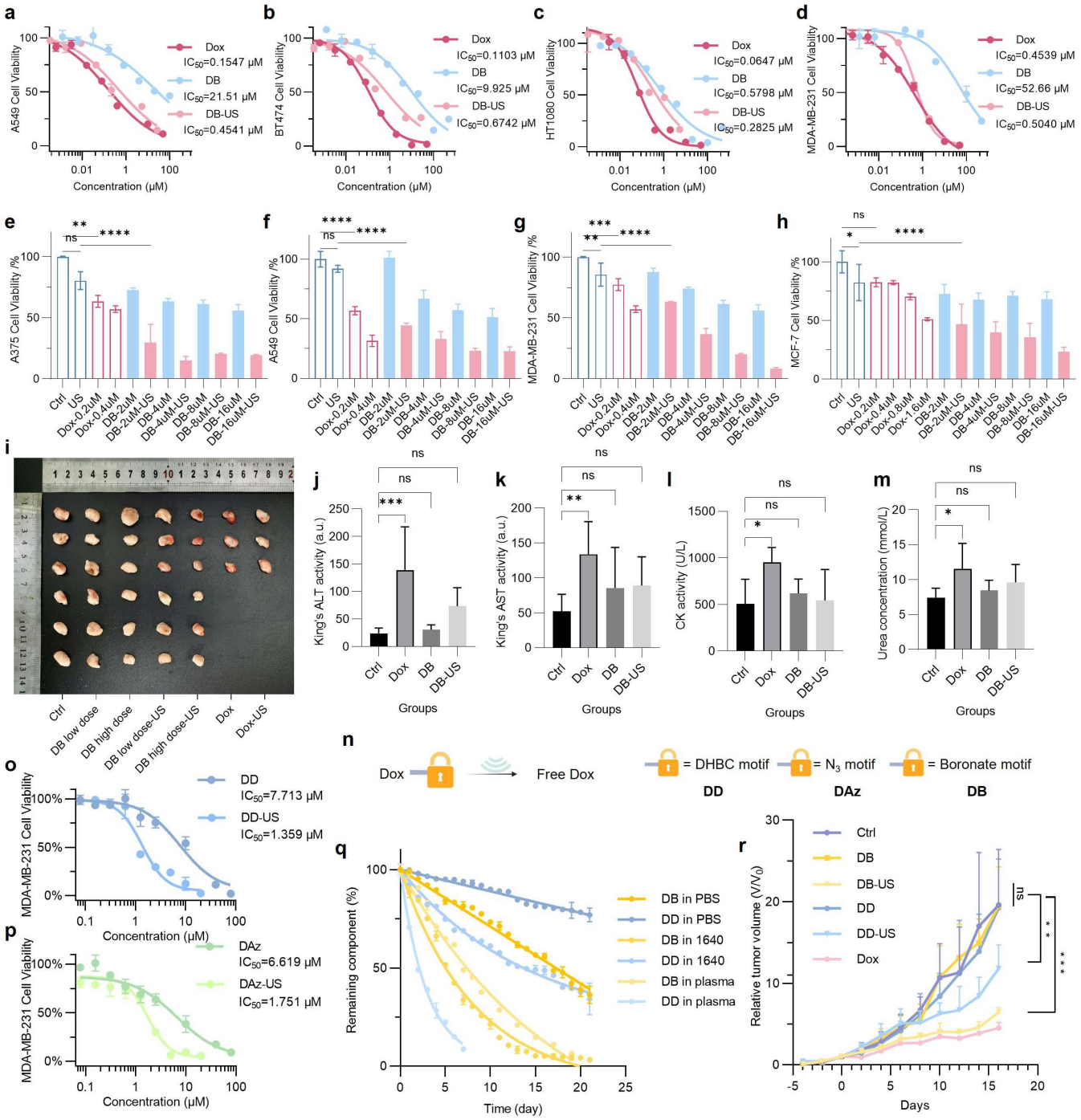


Extended Data Fig. 3 | Additional fluorogenic probe characterization and activation under complex chemical environments. a, US irradiation of two 'fluorescence-caged' probes CB and MRB results in fluorescence turn-on. **b–d**, Ultrasound-triggered activation of CB. **b**, Time-dependent conversion of CB (10 μM in 0.02 M PBS buffer, pH7.2) into 7,4-Hfc under ultrasound irradiation. **c,** HPLC traces showing CB (R_T= 5.20 min) consumption and 7,4-Hfc (R_T = 3.62 min) formation after increasing ultrasound exposure. **d,** Fluorescence emission spectra of CB after ultrasound treatment. **e–g,**

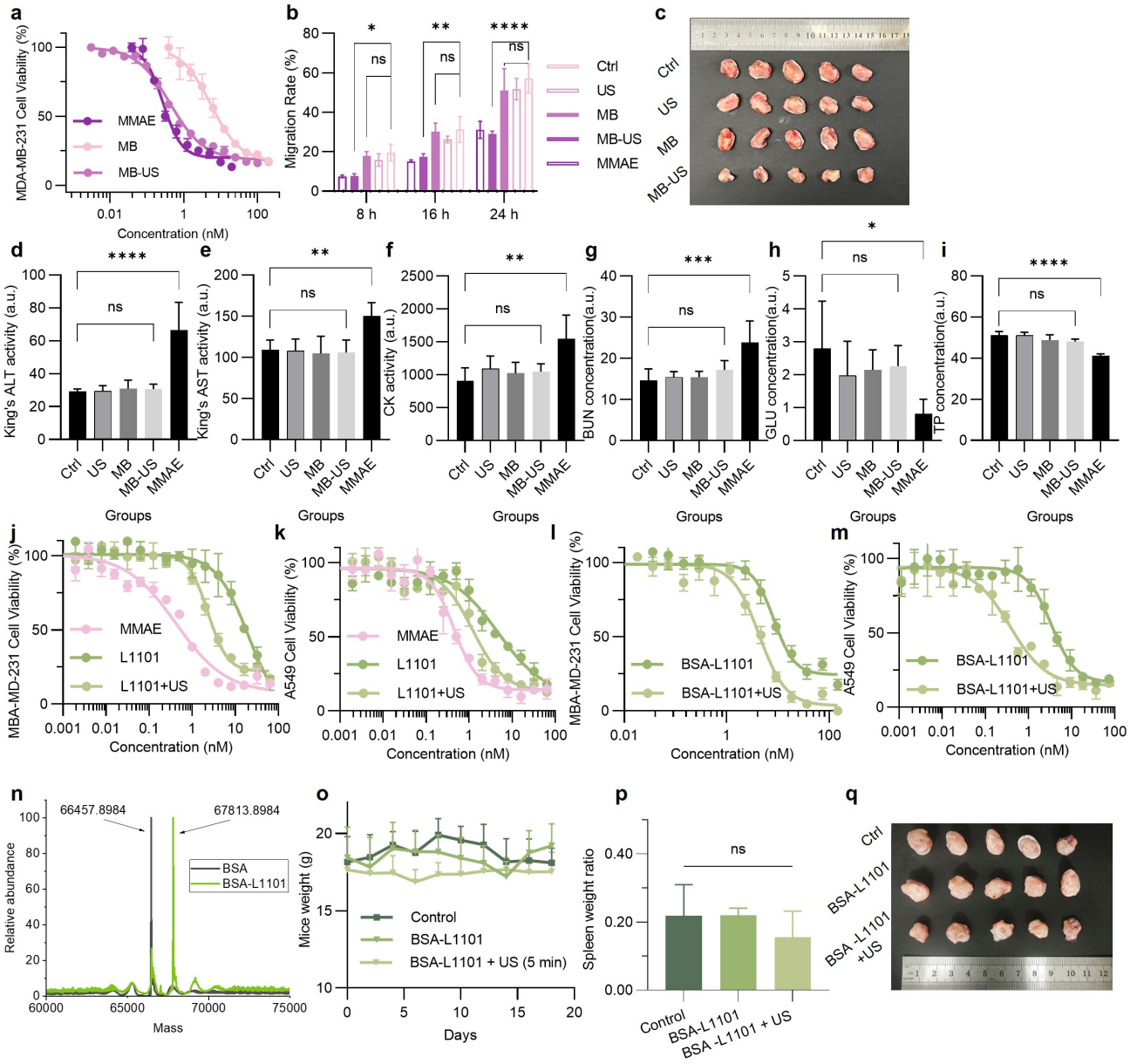
Ultrasound-triggered activation of MRB. e, Time-dependent conversion of MRB (10 μM in 0.02 M PBS buffer, pH7.2) into MR under ultrasound irradiation. **f,** HPLC traces showing MRB (R_T = 6.57 min) consumption and MR (R_T = 3.78 min) formation after increasing ultrasound exposure. **g,** Fluorescence characterization of MRB activation under ultrasound. **h-i**, Selectivity of ultrasound-triggered CB activation in PBS and under reductive conditions. The boronic acid-caged probe CB is preferentially activated by H_2O_2 and ultrasound relative to other ROS in PBS. And the selective reactivity of the boronic acid masking group to ultrasound is even more pronounced under reductive conditions (GSH 10 mM). **j-k**, Comparison of ultrasound-triggered and H_2O_2-triggered CB activation in PBS and in DMEM containing 1 mM GSH. Ultrasound-triggered activation proceeds more effectively than exogenous H_2O_2 in reductive media, supporting the additional advantages of ultrasound over hydrogen peroxide activation in biologically relevant systems. **l-n**, Conversion kinetics of CB (10 μM) under ultrasound irradiation in complex environments (l, PBS; m, DMEM + 10% FBS + GSH 1mM; n, cell lysate, pH 6.5). Ultrasound-triggered activation consistently shows efficient fluorescence turn-on in various complex environment, demonstrating tolerance to biologically relevant environments.



Extended Data Fig. 4 | Additional cellular and tumour imaging validation of ultrasound-triggered probe activation. a, Confocal fluorescence imaging of CB (10 μM) activation in MDA-MB-231 cells under in situ ultrasound irradiation. **b**, Confocal fluorescence imaging of MRB (10 μM) activation in MDA-MB-231 cells under in situ ultrasound irradiation (Hoechst 33342 (5 μM) was used for nuclear staining.). **c**, Flow-cytometric analysis of MRB (10 μM) activation in MDA-MB-231 cells. **d-e**, Ex vivo imaging of ultrasound-triggered MRB activation in tumours from 4T1 tumour-bearing mice. The mice were intratumourally given MRB (0.3 mg/kg) and then received ultrasound irradiation (2.5 W/cm^2, 70% duty cycle).



Extended Data Fig. 5 | Additional cellular and in vivo validation of ultrasound-triggered doxorubicin prodrug activation. a–d, Cytotoxicity assays of DB in multiple cell lines. The prodrug was irradiated under in vitro ultrasound (3.0 W/cm^2, 70% duty cycle, 3 min). **e–h,** Cytotoxicity assays of DB in multiple cell lines under cell-compatible ultrasound conditions. The prodrug was irradiated under in situ ultrasound (1.0 W/cm^2, 10% duty cycle, 5 min). **i**, Endpoint tumour-volume analysis in 4T1 tumour-bearing mice treated with DB and ultrasound. Dox group had 3 mice sacrificed for exceeding 20% weight loss on day 11 (n = 3 on day 14). **j–m**, Blood biochemical analyses after DB treatment in vivo.



Extended Data Fig. 6 | Additional cellular and in vivo validation of ultrasound-triggered MMAE prodrug and conjugate activation. a-b, In vitro and in situ cytotoxicity assays of MMAE prodrug MB in MDA-MB-231 cells. **c**, Endpoint tumour-volume analysis in 4T1 tumour-bearing mice treated with MB and ultrasound. **d–i**, Blood biochemical and hematological analyses after MB treatment in vivo. **j-k**, Cytotoxicity assays of L1101 in multiple cell lines under ultrasound treatment. **l-m**, Cytotoxicity assays of the BSA-L1101 conjugate in multiple cell lines under ultrasound treatment. **n**, Body weight changes in 4T1 tumour-bearing nude mice treated with BSA-L1101 and ultrasound. **o**, Spleen weight ratio (spleen weight/body weight, a.u.) comparison at the endpoint of BSA-L1101 treatment. **p**, Endpoint tumour-volume analysis in mice treated with BSA-L1101 and ultrasound.

Supplementary Files

This is a list of supplementary files associated with this preprint. Click to download.

- Supplementaryinformation.pdf